World line dependence of current sheet normals inferred by minimum variance techniques

J. D. Scudder and Z.-W. Ma
Department of Physics and Astronomy, University of Iowa, Iowa City, Iowa, USA

N. Omidi
Department of Electrical Engineering, University of California, San Diego, La Jolla, California, USA

P. Puhl-Quinn
Institute for the Study of Earth, Oceans, and Space (EOS), University of New Hampshire, Durham, New Hampshire, USA

Received 2 July 2004; revised 23 November 2004; accepted 9 February 2005; published 6 August 2005.

[1] The reconstruction of current sheet geometry is investigated as a function of paths through an oblique two-dimensional (2-D) hybrid supercritical shock and two fluid simulations of the magnetopause with no, small, and large guide fields, respectively. For world lines near the separator or 2-D structures in shocks, systematic errors swamp statistical ones tenfold. The systematic angular errors of the magnetopause surface normal determined by minimum variance analysis (MVA) using >100,000 world lines are contrasted with recommended statistical error cones. The systematic errors range as high as 90° but typically more than 20°. Errors do not have a most probable value at the magnetopause when using MVA on the magnetic data, MnVA(**B**), and remain substantial when the Faraday residue, MnVA(FR), is minimized. The 68% confidence error on MnVA(FR) normals is 0–15°. "Skimming" world lines oblique to the current sheet normal are the most susceptible to the MnVA(**B**) and MnVA(FR) systematic errors discussed here, whether or not the world line pierces the separator. MnVA(**B**) almost always erroneously insists that a guide field is present when none is present in the simulation. MnVA(FR) does a better job at guide field recovery, although it too can be error prone. Similar issues are demonstrated for oblique world lines through a 2-D hybrid simulation of an oblique supercritical shock. Shock normal systematic errors are 35° and 20° at the 68% confidence for MnVA(**B**) and MnVA(FR), respectively. The eigenvalue ratios that accompany the least error prone MnVA(FR) reconstructions usually satisfy $\lambda_2/\lambda_1 > 10$. Eigenvalue ratios for MVA(**B**) are rarely this large, and the errors reported here reflect this circumstance.

Citation: Scudder, J. D., Z.-W. Ma, N. Omidi, and P. Puhl-Quinn (2005), World line dependence of current sheet normals inferred by minimum variance techniques, *J. Geophys. Res.*, *110*, A08201, doi:10.1029/2004JA010661.

1. Introduction

[2] The orientation and speed of "free" surfaces in space plasmas are often inferred assuming the recorded variations are caused by layers of one spatial dimension moving past the observer. Techniques of this type in the literature that determine the orientation and speed of such layers are Rankine-Hugoniot [*Viñas and Scudder*, 1986], Faraday residue [*Terasawa et al.*, 1996; *Khrabrov and Sonnerup*, 1998] and normal mass flux variance [*Sonnerup et al.*, 2004], which generalize the original Minimum variance analysis, MVA(**B**), applied to the vector magnetic field data [*Sonnerup and Cahill*, 1968]. In recent years there are additional techniques attempting to reconstruct two-dimensional features of these layers from a single spacecraft [*Hau and Sonnerup*, 1999] and the multiple spacecraft techniques with Cluster. Without a current sheet normal the phase speed of the surface cannot be determined, the Poynting flux into the current sheet cannot be calculated, the reconnection rate cannot be determined, and the spatial scales of the layer interior cannot be reconstructed from the time series measurements. The three-dimensional orientation of the local "natural", or "boundary normal" coordinate system must be available before an informed decision can be made whether the local data support the antiparallel or component reconnection scenario. These difficult inversions of the time series into geometry, even if done flawlessly, only partially determine the variables that affect the recorded time series through the layer. Among the most unexplored variables are those that control which vectors are sampled one after another, and, in fact, determine the

0148-0227/05/2004JA010661$09.00

magnitude and orientation of the electric and velocity vectors recorded at the spacecraft. These variables are those that define the motion in space and time of the spacecraft relative to the layer; they are succinctly described as those that determine the "world line" of the observer. The three techniques above that determine relative motion only determine the layer's speed along its normal and are silent about both the observer's relative motion transverse to the normal and the absolute position along the layer surface where the spacecraft actually pierces the layer. If the layer is truly 1-D these ambiguities cause no difficulties and contribute nothing to the time series recorded on the spacecraft. However, real boundary layers in space possess transverse gradient scales, whether they arise from separator physics, finite radius of curvature, surface waves or finite Larmor radius corrugations. Accordingly, any given time series across such a layer has embedded variations that *can* compromise a time to geometry inversion predicated on the layer's being one-dimensional. Issues such as the location of the world line relative to special structures in the layer (such as the separator, a minimax in a surface wave, or an especially intense overshoot in the shock layer) cannot in principle be determined even when "the" correct boundary normal system is known. The tangential relative velocity of the observer also determines what fraction of the time samples have embedded information of transverse structures that may be present.

[3] Thus each time series is associated with a world line parameterized by two unknowable parameters. In this paper we survey the same, physically realistic, resolved current layers along many different world lines indexed by these "unknowable" parameters to elucidate the intrinsic uncertainty of recovery of the "true natural coordinate system"; from this systematic ambiguity flows a range of uncertainties about theoretically desirable quantities about the layer, including the reconnection rate, the size of the guide field, the size of the mass flux through the layer as well as other quantities such as the scale size of structures traversed. The present study quantifies the size and variation of the systematic errors on the normal, the tangential electric field and the guide field that reflect the possible spectrum of unknown world line variables compatible with those properties that are knowable.

[4] In this way we also provide an estimate of the systematic ambiguities of derived quantities such as the guide field or tangential electric field that are controlled by the geometrical reconstruction errors. The explicit and controlled calculation of these errors provides a quantitative reminder that "transforming to the minimum variance frame" should not be casually done without as many cross checks as the data set may allow. Failing these cross checks, the sizes of systematic angular errors for inferred "special" directions in the layer must be increased by more than an order of magnitude relative to those implied by the "random" error estimates that ensue from considerations of the eigenvalue spread. Finally, since the normal determination is only part of the final determination of a boundary layer coordinate system, it should be clear that questions involving the projection of some observed vector along a given, but only inferred, direction or plane are particularly imprecise. For example, the presence or absence of a guide field, hinge on inferring the size of such projections. Even the simple issue of determining the size and sign of the normal component of **B** at the magnetopause current layer is only as good as this coordinate system. Determining the reconnection rate by determining the tangential electric field, $\mathbf{E}_T = \mathbf{E} \cdot (\mathbf{I} - \hat{\mathbf{n}}\hat{\mathbf{n}})$, has a similar difficulty, as does the direct measurement of the component of plasma inflow velocity in the current layer's rest frame. The quality of all these theoretically interesting quantities are only as good as the determination of the basis vectors of the boundary layer coordinate system. While the traditional mathematical machinery used for such coordinate systems always give answers, the quality of those answers is not always high.

[5] Throughout this paper we will refer to two techniques: minimum variance analysis, MnVA, and maximum variance analysis, MxVA. When referring to both we will revert to MVA. The theoretical foundation for MnVA rests on conservation laws through layers that have spatial variations in only one (to be found) direction and are presumed time stationary. The MnVA was initially formulated for use with the magnetic field alone [*Sonnerup and Cahill*, 1968]. This technique will be denoted MnVA(**B**). Minimum variance is also involved in the Faraday residue analysis, MnVA(FR), using $\mathbf{E}'$ and $\mathbf{B}'$ data collected in the same frame of reference [*Terasawa et al.*, 1996; *Khrabrov and Sonnerup*, 1998]. This technique involves a generalization of the approach studied earlier by *Sonnerup et al.* [1987, 1990], who formulated the moving layer problem by searching for a transformation to the deHoffmann-Teller frame and extremizing MxVA($\mathbf{E}^{\mathrm{HT}}$) to define the normal, while essentially using the MxVA(B) to define the orthogonal basis vector. The electric field observed in the spacecraft frame has also been used directly with MxVA; when such analysis is used it will be referred to as MxVA($\mathbf{E}'$). Since the electric field is not a Galilean invariant, care must be taken when referring to MVA techniques involving **E**. We will refer to the electric field measured in the spacecraft frame as $\mathbf{E}'$, and the electric field in the rest frame of a propagating structure as **E**.

[6] Previously three classes of difficulties in MVA have been discussed: (1) sensitivity of the eigenvalue-eigenvector algebra to random error, such as digitization error or other white noise sources, (2) the separation of the eigenvalues and nonuniqueness of the basis in which the variance is diagonal, and (3) various aspects of nonstationarity $\partial \mathrm{B}/\partial t \neq 0$. Formulae for estimating sensitivities to uncertainties of the first two types have recently been summarized [*Sonnerup and Scheible*, 1998]. Various recipes have also been advocated for the third class of problems, including averaging nearest neighbors, filtering the data against "unwanted" high frequency waves, or removing substructure of the layer [cf. *Sonnerup and Scheible*,1998]. Unfortunately, such procedures presume that the user has "a priori" knowledge concerning layer substructure in the time records and can excise the $\partial \mathrm{B}/\partial t \neq 0$ structures so that the truly time stationary content of the layer is preserved. This editing must be done carefully (if at all) to not upset the relative variance of each of the components from the true spatial variances that the unknown layer would have had in the absence of the nonstationary behavior.

[7] Two further complications that have received virtually no attention in the MVA context are (1) the use of proxy values for $\mathbf{E}'$ when three axis measurements of $\mathbf{E}'$ have not

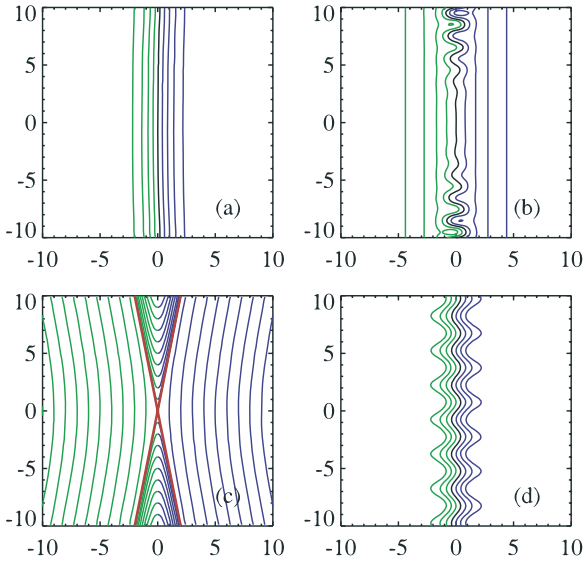

Figure 1. Various ways to break 1-D approximations at boundaries: (a) weakly, with no internal structure and large radius of curvature; (b) asymptotically weak violation, with nested higher-dimensional variation confined to the layer; (c) singular variant of Figure 1b such as near the separator of magnetic reconnection; (d) gross violation of the 1-D approximation.

been made and (2) the quantitative influence of nonplanar current sheets on the accuracy of these techniques. In the absence of $\mathbf{E}'$, calculations of the unipolar electric field from ion flow and magnetic field measurements have on occasion been substituted [*Paschmann et al.*, 1986; *Sonnerup et al.*, 1987, 1990]. When three axis electric measurements were not made, the spin axis component of $\mathbf{E}'$ has been synthesized presuming $\mathbf{E}' \cdot \mathbf{B}' = 0$ or worked around [*Aggson et al.*, 1983]. To examine the first class of issues requires a specific approximation for $\mathbf{E}'$ to be considered and must be done on a case by case basis. In the second category various authors use MVA techniques presuming that it determines the local, average normal to a possibly wavy surface. All free surfaces in space have some degree of variation in the direction transverse to the "true" normal; such variations are "outside the MVA model."

[8] In this paper we explore the systematic errors associated with determining normals (and related coordinate systems) as if the layers traversed were one-dimensional, even though the layers are physically consistent models of the magnetohydrodynamics and contain spatial variations in two dimensions. These systematic issues are intrinsic to the physical problem of deducing the "natural" coordinate system from a time series of perfect three-dimensional local measurements of the electromagnetic field. Various relaxations of the 1-D layer approximation are illustrated in Figure 1. Figure 1a illustrates an ideal, large radius of curvature free surface with negligible thickness. Figure 1b illustrates one level of complication on the situation of Figure 1a: far from the actual transition the medium is one-dimensional but contains two-dimensional, or even three-dimensional, structures internal to the layer. These structures may be associated with the maintenance of the layer as with shock overshoots in supercritical shocks, finite Larmor radius features or surface waves. Surface waves have been posited on the magnetopause, possibly as a result of Kelvin-Helmholtz instabilities. Hybrid codes resolving the physics of the magnetopause/shock layers reveal finite Larmor radius substructures that will be sampled on a given pass by spacecraft. Gyrating ions support two-dimensionally structured density and magnetic field overshoots in supercritical shock waves behind the main current ramp of the shock with scale sizes comparable to the convected ion inertial length. Such phenomena have been inferred in supercritical shock layer studies [*Scudder et al.*, 1986] and also seen in 2-D Hybrid simulations of supercritical shock waves [*McKean et al.*, 1995]. Presumably all transitions in space physics have finite ion Larmor radius substructures that produce an admixture of irreducible 2-D effects. Figure 1c presents a schematic section of separatrix layers near a reconnection site. Such a regime has half-spaces where the current layers are quasi 1-D, but a portion of the layer contains explicitly two-dimensional variations. In particular, the x component of the magnetic field (parallel to the global normal) reverses sign in this region presenting $\partial B_x/\partial x \neq 0$, reflecting the two dimensionality of the layer. While $\nabla \cdot \mathbf{B} \equiv \mathbf{0}$ everywhere in these solutions, that null result arises from compensating spatial variations along and transverse to the local normal. At its core MnVA presumes that this null divergence is a corollary to the one-dimensional variation through the layer, and that $B_x = C$, independent of space. The observer's problem then, is just to find the direction where that is true. Neither MnVA(**B**) nor MnVA(FR) will be free from systematic errors that ensue when these techniques are used in the vicinity of the separator. The observer who does not cross the separator regime, but crosses the current layer at a large angle to the normal, will also record a spatially varying component of **B** along the global normal; MnVA(**B**) proceeds to choose a normal that will reduce this intercepted variance as best it can, by reorienting the normal. Information such as this that is outside the posited 1-D layer model of MVA is unavoidably folded into the normal selected by MVA and can distort the reported morphology of Θ_{Bn} dependencies determined using this technique [e.g., *Meziane et al.*, 2002]. Finally, Figure 1d illustrates a transition that is not locally planar on either outer or inner scale.

[9] With the evolving Polar, Geotail, Cluster and proposed MMS orbits, skimming trajectories oblique to the local free surface normals have become more commonplace. As shown below, the larger this angle, the larger the expected systematic error on MVA normals. The fully defined world line of the observer determines what effects of the higher dimensionality of the current sheet are embedded in the time series used for MVA.

[10] While statistical analysis of large suites of current layers can discard layers that do not "cooperate" with the 1-D preconditions of MVA, there remains the ongoing use of MVA for boundary coordinates for "singular" case studies where analysis "must" go forward [e.g., *Mozer et al.*, 2002]. If such a "unique" magnetopause crossing has ideal instrument coverage with appropriate time resolution and is a "textbook" example needing such a coordinate system, how far should the quantitative analysis of the data proceed as if the normal is that determined by MnVA(**B**) and associated random error cones determined from

eigenvalue analysis? Are the random error bounds of this "inverse" model so reliable that other measurements suggesting a slightly different normal outside the MnVA(**B**) error cones should be discarded? Is the selection of a MnVA coordinate system that has normal component of **B** sensibly "constant" a proof that the layer diagnosed "really is one-dimensional"? Are there warning signs in the data set that are not associated with the MVA proper that can signal the likelihood of large systematic errors? If MnVA(**B**) and MnVA(FR) agree at some level of precision, does this imply that the normal is accurately known to be in the overlapping error cones and the layer planar? Do composite tests, like MnVA(FR), that involve electric and magnetic fields surmount this problem, or are they as weak as their weakest link? We propose to shed some light on this and related problems by solving the associated "forward" problems at theoretically complete magnetopause and shock current layers, contrasting the MnVA normals with the normals known to the simulators of these layers. In this way we will map the systematic errors of the MnVA inversion process itself, having an absolute control on the direction of the normal.

[11] A critical discussion of the background of minimum variance techniques and their generalizations is summarized in Appendix A. There the close relationship between the variance matrix and the moment of inertia matrix from classical mechanics is developed to given an intuitive feel for the nature of the approximations involved when using MVA techniques on real boundaries, as if they were one - dimensional ones.

2. Model

[12] The present paper contrasts the true current sheet normal with the MnVA(**B**), MnVA(FR) and the MxVA(**E**) directions determined from time series deduced as an "observer" tours a fully resolved ambipolar, Hall MHD reconnecting current sheet [*Ma and Bhattacharjee*, 1996] or a hybrid model of an oblique supercritical shock layer [*McKean et al.*, 1995]. In this way we determine the systematic errors involved by contrasting the local current sheet boundary normal suggested by MVA with the actual normal known to the global simulation. The present approach differs in two ways from the previous analysis of the MVA approach: (1) a spatially resolved, physically consistent, time stationary current system with a known normal and guide field size is sampled by an observer moving through the structure along a prescribed world line with a velocity **C** inclined at an angle α to the true layer normal. This observer moves along the layer normal with a speed $C_n = C \cos \alpha$; (2) the current layers inventoried contain physically consistent, time stationary, two-dimensional spatial variations of **E**, **B**.

[13] The magnetopause current layer simulations to be used have three variants: those with (1) no guide field, (2) small guide field, and (3) strong guide. The ignorable coordinate in these simulations is the $\hat{\mathbf{y}}$ direction, the direction of the constant (and possibly vanishing) guide field imposed as a boundary condition. The three magnetopause solutions are delineated by $B_y(x = \pm\infty) = [0, 0.1, 1]$ $B_z(x = \infty)$, respectively. The z components of the asymptotic fields are those that are interconnecting, while the $\hat{\mathbf{x}}$ direction in the simulation is the symmetry axis for the plasma inflow and is the true normal direction, $\hat{\mathbf{n}}_{\mathbf{T}}$. Even in the presence of separatrices with finite opening angles, the asymptotic inflow direction is well defined and is the axis along which the reconnection rate is determined and for which the boundary normal is desired.

[14] The rest frame observer's catalogue of the spatial variation of **E** and **B** along a spatial path through the solution are used to construct a "time series" of the electromagnetic field $\mathbf{E}'(t)$, $\mathbf{B}'(t)$ that a spacecraft born sensor would record for subsequent use with MVA. For survey purposes we consider a family of linear spatial paths in the x-z plane as world lines for sampling the solution. The equations of these world lines are parameterized by the angle α between the world line and the true normal, and the intercept Z_o along the current sheet where the world line pierces the current layer. Thus the surveyed paths have equations of the form $z = z_o + x \tan \alpha$. When comparing world lines with different slopes we modify the velocity, **C**, so that the phase speed, C_n, along all world lines is the same.

[15] The electromagnetic field in the rest frame of the simulation was interpolated onto a uniform rectangular mesh spanning the ranges: $|z| \leq 2$ and $|x| \leq 1$, where distances are measured in asymptotic ion inertial lengths, $d_i = c/\omega_{pi}$. The interpolation of the solution onto a mesh effectively replicates the sampling of the field at periodic intervals, guaranteeing that the time profile of the field along the world line does not over sample the regions where the electromagnetic field is strongly varying that required extra grid resolution in the numerical code. Only the world lines that transit the entire x range of the solution along the normal are analyzed. We consider 31 values of $|z_o(i)| < 4$ and 31 equispaced values of α_j. Of these 31×31 possibilities we only examined world lines s_{ij} that satisfied $z_o^2(i) = \tan^2 \alpha\,(j) \leq 4$. Along the world line s_{ij} the spatial sequences of $\mathbf{B}(s_{ij})$ and $\mathbf{E}(s_{ij})$ were catalogued as reported by the steady state output of the computer code. These sequences of the electromagnetic field were then transformed according to Galilean relativity to produce the electromagnetic field that would be recorded on the spacecraft:

$$\mathbf{E}'(s_{ij}) = \mathbf{E}(s_{ij}) + \mathbf{C} \times \mathbf{B}(s_{ij})/\mathrm{c}; \mathbf{B}'(s_{ij}) \simeq \mathrm{B}(s_{ij}).$$

These modified sequences of $\mathbf{E}'$, $\mathbf{B}'$ are now parametrically ordered by the spacecraft observer's clock. Here we recall our convention that the primed $\mathbf{E}'$ fields are those seen on the spacecraft which are different from those recorded by the rest observer in the simulation, **E**. From these transformations it should be clear that for the moving observer the spatial variations of **B** transverse to **C** add correlated spatial variations to each component of $\mathbf{E}'$, so that covariance matrix $\mathbb{C}$ of the MVA technique when used with electric fields (is different in the spacecraft frame than in the layer's rest frame: $\mathbb{C}(\mathbf{E}') \neq \mathbb{C}(\mathbf{E})$, while $\mathbb{C}(\mathbf{B}') \simeq \mathrm{C}(\mathbf{B})$.

[16] Each sequence of the electromagnetic field along its world line s_{ij} determines, via MnVA($\mathbf{B}'$), a proxy current sheet normal $\hat{\mathbf{n}}_B(i, j)$; another proxy normal $\hat{\mathbf{n}}_{FR}(i, j)$ can be obtained via MnVA(FR); and another one, $\hat{\mathbf{n}}_{E'}(i, j, \mathbf{C})$, via MxVA($\mathbf{E}'(s_{ij})$, **C**). The variance matrices and the inferred proxy normals will change as the world line specification s_{ij}

and relative velocity, **C**, change. Having established how the pseudo spacecraft data **E**′, **B**′ sequences are determined from the spatial variation of the simulation's (**E**, **B**) and the world line of the observer, we suppress the primes in the subsequent discussion. Unless noted otherwise all subsequent analysis using MVA is performed on quantities as they could be observed on the moving spacecraft.

[17] Since the true normal, $\hat{\mathbf{n}}_T$, to the current sheet is known from the simulation, we also record the angular deviations of the various proxy normals, $\hat{\mathbf{n}}_\ell$, $\ell = \{B, FR, E'\}$ from the true normal $\delta\theta_\ell = \cos^{-1} \hat{\mathbf{n}}_\ell \cdot \hat{\mathbf{n}}_T$ for each world line s_{ij} and choice of front phase velocity. Of auxiliary interest are the deflections of the proxy normals in the X-Y and X-Z planes given by

$$\delta\theta_{\ell,X-Y} = \tan^{-1} \frac{\hat{\mathbf{n}}_\ell \cdot \hat{\mathbf{y}}_T}{\hat{\mathbf{n}}_\ell \cdot \hat{\mathbf{n}}_\mathbf{T}}$$

$$\delta\theta_{\ell,X-Z} = \tan^{-1} \frac{\hat{\mathbf{n}}_\ell \cdot \hat{\mathbf{z}}}{\hat{\mathbf{n}}_\ell \cdot \hat{\mathbf{n}}_\mathbf{T}}.$$

[18] For the data collected on each world line s_{ij}, C_n we have also determined the recommended maximum half angle of the random error cone about the MVA normal direction for each $\hat{\mathbf{n}}_\ell$ [*Sonnerup and Scheible*, 1998; *Khrabrov and Sonnerup*, 1998], labeling them $\Delta\theta^\ell_{K-S}(i, j)$. These three quantities are then used to scale the size of our detected systematic errors.

[19] With the inferred eigenvectors, $\hat{\varepsilon}^\ell_j$ in hand, we have also routinely checked the reverse diagnosis of the guide field that such analysis would infer by recording $B^\ell_2(t) = \hat{\varepsilon}^\ell_2 \cdot \mathbf{B}(t)$. Because the Hall effect perturbations are normally seen along this or similar directions, we form $\Delta\Upsilon^\ell$, the difference of the time average of B^ℓ_2 and the known asymptotic guide field along the true y, guide, direction, $B_y(x = \infty)$, in units of the variance of B^ℓ_2 about the average which we will denote as σB^ℓ_2, obtaining

$$\Delta\Upsilon^\ell \equiv \frac{\langle B^\ell_2(t)\rangle - B_y(x=\infty)}{\sigma B^\ell_2}.$$

[20] With MnVA(FR) we similarly inventory the errors in the inferred size of the tangential (reconnection) electric field strength in the layer's frame as

$$\Delta\Xi \equiv \frac{|\mathbf{E_T}(MnVA(FR)) - \mathbf{E_T}(x=\infty)|}{\sigma|\mathbf{E_T}|}.$$

[21] Finally, the above process was repeated for each guide field solution at 8 phase speeds C_n = {0.1, 1, 3, 5, 10, 15, 30, 50} km/s for all angles α and intercepts z_o permitted. A similar, but less extensive diagnosis of varying world line parameters, is discussed below for a hybrid code's description of an oblique supercritical shock layer.

3. Results

3.1. Modeled Magnetopause Current Layers: MnVA(B)

[22] To summarize, the over 100,000 MVA analyses performed on these magnetopause and shock layers we establish a format for subsequent figures using the no guide field model of the magnetopause as our first example. Figure 2 shows color-coded matrices $W_{ij}(C_n)$, whose i, j indices label the spatial locus of the world line, s_{ij}, where **E** and **B** were sampled while moving at a uniform speed chosen for this example to be C_n = 15 km/s. The variation of an MVA attribute, here generically called W, is indicated by the color coding of W_{ij} at each pixel location. The W quantities color coded are $\Delta\theta_B(i, j)$ (Figure 2a), $\Delta\theta_{B,X\_Z}(i, j)$ (Figure 2b), $\frac{\max|\mathbf{B}(s_{ij})|}{\min|\mathbf{B}(s_{ij})|}$ (Figure 2c), and $\Delta\theta_{B,X\_Y}(i, j)$ (Figure 2d), as previously defined above. The gray portions correspond to world lines that do not satisfy our traversal constraints summarized above.

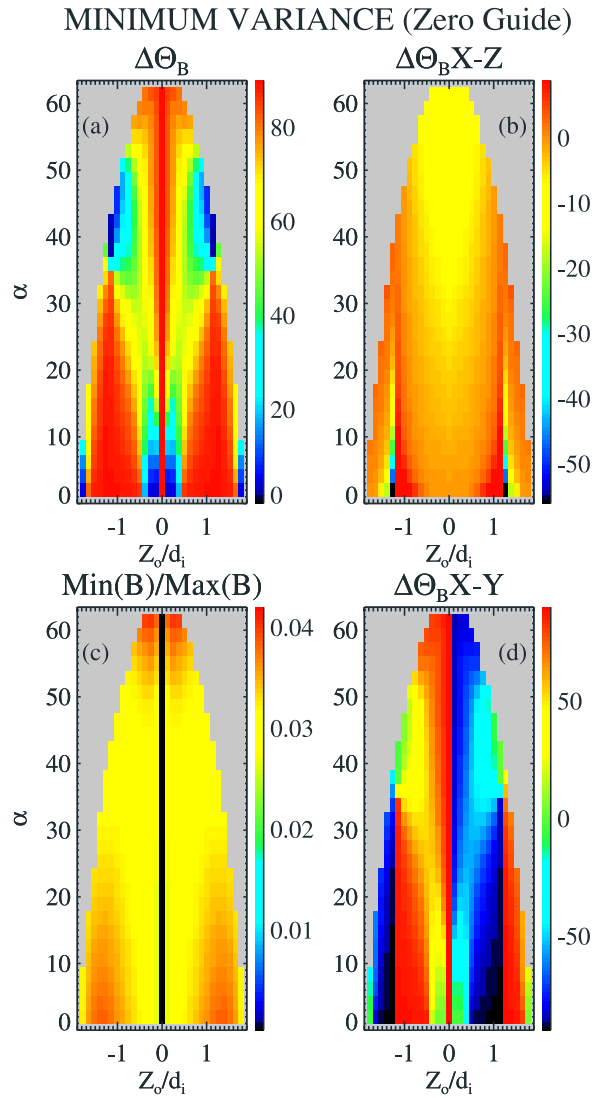

Figure 2. Overview of systematic errors in normals derived from MnVA(**B**) along a spectrum of world lines. C_n = 15 km/s.

[23] In Figure 2a, there are many world lines where the disagreement, $\Delta\theta_B$, between the MnVA(B) $\hat{\mathbf{n}}_\mathbf{B}$ and the true normal to the current sheet exceed 20°; sometimes this disagreement is as large as 90° with all values in between.

Particularly good agreement occurs for $\alpha \simeq 0$, world lines that make a shallow angle with the true normal (provided that they also do not go too close to the separator, $z_o \simeq 0$). Even for normal incidence the Hall magnetic signatures together with the transverse gradients in the true normal component of the magnetic field disturb the normal recovery. Similarly, the world lines that go through the separator sense serious transverse gradients and the normals for MnVA(**B**) are invariably unreliable. Referring to Figure 1c, it is clear that such trajectories contain substantial variations at odds with the 1-D premise of MnVA(**B**). Figures 2b and 2d illustrate that these disagreements are caused by the inferred MnVA(**B**) normal canting toward the $\pm\hat{\mathbf{y}}$, (out of plane, ignorable) directions of the simulation. The error of the MnVA normal is primarily a reflection of variations of $\Delta\theta_{B,X-Y}$, with only modest deflections in the X-Z panel of Figure 2b. The reason for this asymmetry in the aberration of the MVA normal from the true normal stems from the anchoring nature of the Z direction as essentially that of the maximum variance across layers with strong magnetic shear. Because the strongest variation of **B** at the magnetopause in these examples involves the interconnecting and reversing components (except in the strong guide field case), sampling its complete reversal (while the guide field remains steady) virtually dictates the direction of maximum variation direction will be along the $\hat{\mathbf{z}}$ direction of the simulation. Although the asymptotic tangential component of **B** at shock waves do not reverse, they are preferentially weakened or strengthened, identifying the $\hat{\epsilon}_3 \approx \hat{\mathbf{z}}$ direction (except for quasi-parallel shocks) as one of strong variation. What remains unspecific is the selection of "the" minimum variation direction from the infinite number possible in the plane perpendicular to the maximum variance eigenvector. This second direction, and hence the "normal" direction usually inferred from it, is only computationally unique when the minimum and intermediate eigenvalue are well separated. As we have argued the MxVA(**B**) direction is well defined, so this comparison of eigenvalues comes down to the variance along the true normal (witnessed along the actual world line) versus the variance of the components of **B** (witnessed along the actual world line) generally in the $\hat{\mathbf{y}}$ direction. When the world line passes through layers where $B_x = f(z)$, as near the separator, the search for the minimum variance direction cants into the third, and relatively unconstrained $\hat{\mathbf{y}}$ direction to minimize the variance. As shown below the layer variance in $B_y = h(x)$ in shocks "resists" this tendency, assisting MnVA(**B**) normals at shocks to fortuitously be more precise, overall, than the magnetopause. Nonetheless, even at shocks as shown below they are not of high quality, and frequently shock geometry is determined using blunt body models, rather than local normals from techniques like MnVA.

[24] The slight deflections of the proxy normal indicated in Figure 2b reflect the small deviation, (~5°) of the MxVA(B), eigenvector as determined by all these world lines; by contrast, the large deflections indicated in Figure 2d reflect the vagaries of actually picking a direction, $\hat{\epsilon}_1$ within the plane perpendicular to $\hat{\epsilon}_3$ that minimizes the variance projection as seen along the peculiar world line folded into the minimum variance matrix, $\mathbb{C}$.

[25] Figure 2c indicates that it is not possible by considering the variation of $|\mathbf{B}|$ seen along the world line

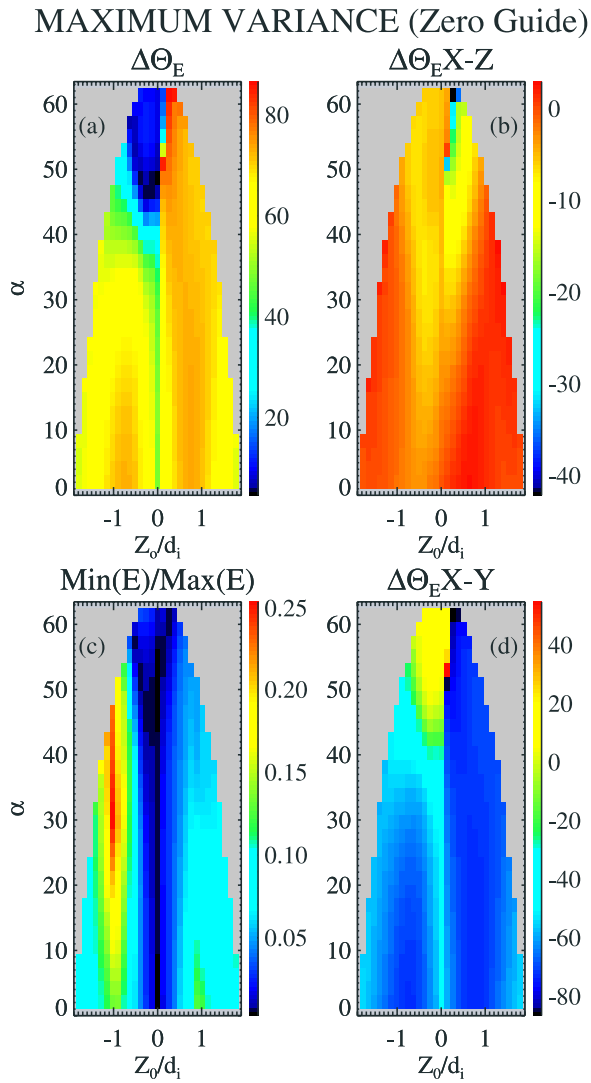

Figure 3. Overview of systematic errors using MxVA($\mathbf{E}'$) along the same world line trajectories as in Figure 2, but from the wrong (i.e., spacecraft) frame, moving with C_n = 15 km/s along the normal.

to differentiate which world lines give higher quality normals than others. If reconnection proceeds at a null point with no guide field, clearly such world lines will advertise this circumstance with high magnetic field intensity contrast along them. (However, a further complication is that an ideal rotational discontinuity can produce layers where the magnitude of B varies in the presence of pressure anisotropy, without being near the separator [cf. *Hudson*, 1970].) Such world lines are expected to have high degrees of spatial variation transverse to the normal. However, one may not invert this argument to say because $|\mathbf{B}|$ does not vary strongly that the world line is far removed from the separator and strong transverse scales since with a guide field the separator could have been penetrated without a strong contrast in the field's magnitude. Additional sources of intrinsic two dimensionality at the magnetopause are the expected quadrupolar, Hall MHD, perturbations of the magnetic components out of the x-z plane, which also have spatial dependence in the

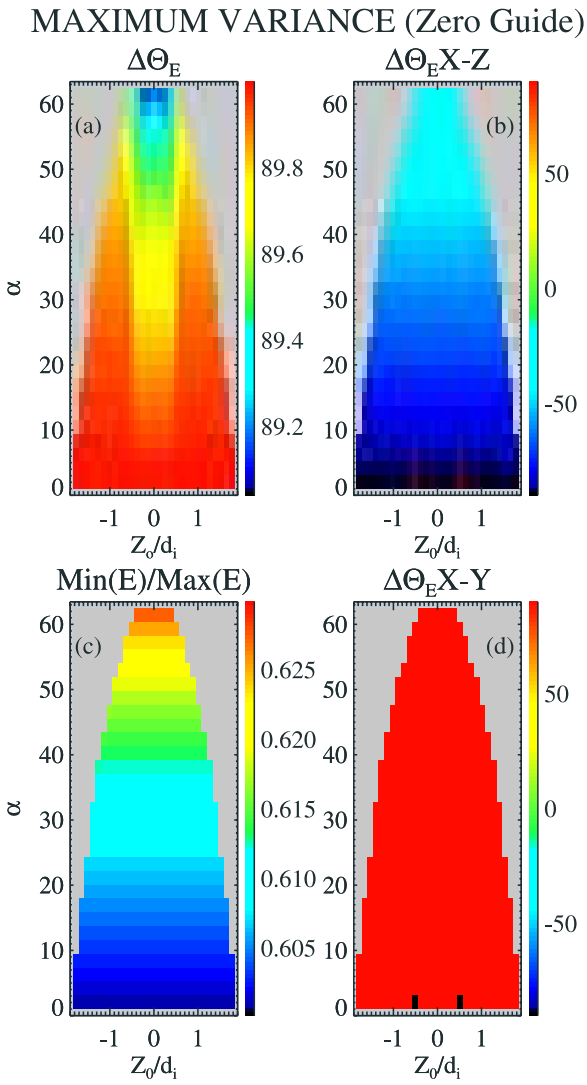

Figure 4. Overview of systematic errors using MxVA($\mathbf{E}'$) along the same world line trajectories as in Figure 2, but examining a resolved truly 1-D rotational discontinuity structure, but from the wrong (i.e., spacecraft) frame. C_n = 15 km/s.

X-Z plane. Hence any oblique world line to the normal passing with $|z_o| \leq O(c/\omega_{pi})$ will sense this variation (required to make it a quadrupolar pattern) and locate the minimum variation direction as a tradeoff between catching the variation of $B_x(z)$ in one extreme or $B_y(z)$ in the other.

[26] Figure 2 illustrates that the path of the observer's world line does determine different admixtures of 2-D effects embedded in the variance matrix, which, in turn, impact the quality of the inferred normal. Accordingly, the possible errors in the normal on any given time series could be as large as the largest mistakes illustrated in Figure 2a, i.e., 90°. Below we summarize the distribution of such normals, illustrating for the magnetopause that the probability for getting the correct normal via MnVA(**B**) is very flat, with no "typical" systematic error that should be considered on any given world line.

3.2. Modeled Magnetopause Layers MxVA($\mathbf{E}'$)

[27] Figure 3 illustrates the results of MxVA($\mathbf{E}'$) in the same format as Figure 2 as performed on the electric field, $\mathbf{E}'$, available in the spacecraft frame. While Figure 3 does illustrate some world lines that pierce the separator nearly along the normal where the maximum variance eigenvector is as close as 20° to the true normal, this precision is atypical. This fortuitous agreement occurs since the magnetic field along these paths is so weak that the Galilean corrections present in $\mathbf{E}'$ are not as substantial as occur for other world line paths. For almost all other world line geometries the error in the normal determination is so prohibitively large to make this technique worthless!

[28] To clarify the role of 2-D effects versus the (inappropriate) analysis of $\mathbf{E}'$ (as if it were **E**), we have conducted the same MxVA analyses on a truly 1-D variation model of a RD with a finite transition layer. The data are acquired moving with the same relative speed C_n = 15 km/s for the same range of world lines as in Figure 2; the errors in the inferred normals are summarized in Figure 4. By construction there are no spatial variations in the modeled layer transverse to the normal; as seen in Figure 4, all W_{ij} entries are (essentially) independent of the intercept of the trajectory (small differences reflect different numbers of data points depending on z_o, while world lines of different inclinations, α, at constant C_n are traversed with different speeds, so that the departure of the $\mathbf{E}'$ data from the rest frame **E** is almost exclusively organized with α which determines the final orientation of **C**. All of the errors $\Delta\theta_{E'}$ of this MxVA($\mathbf{E}'$) from the true normal are attributable to the analyzed data having been collected in the wrong frame relative to the rest frame of the 1-D spatial structure. As can be seen these effects are a primary factor in the normal errors, while the 2-D effects illustrated in Figure 3 add structure to the errors as a function of intercept of the trajectory relative to the separator. In any case the use of MxVA($\mathbf{E}'$) at RD, TD or oblique shock layers (with visible sheer in **B**) is a broken lever.

3.3. Modeled Magnetopause Layers: MVA With Electromagnetic Field (MnVA(FR))

[29] The MnVA(FR) technique is, however, designed to compensate for $\mathbf{E}'$ data having been collected in a frame that is not the rest frame of the current layer. This technique simultaneously determines the optimal frame transformation speed along the normal, C_n, while also estimating the normal direction. We illustrate in Figure 5 the errors by this technique in the recovery of the normal direction at the same 2-D no-guide model that underlies Figure 2 of the magnetopause. Since the Faraday residue technique strives to minimize the variation about an optimal choice of minimum variance of **B** and of minimum variance about the choice of $\mathbf{E}_T$ in the layer's rest frame, we might anticipate better normal recovery of the layer properties with MnVA(FR) in the presence of 2-D effects than with MnVA(**B**) alone. This is illustrated in Figure 5a, where the Faraday residue normal errors are usually less than 20° and, in Figure 5c, within 45% of the true relative speed of propagation. Figures 5b and 5d show, however, the same bias to the errors of the normal as seen in the MnVA(**B**) survey of Figure 2, with the error in the X-Y plane 7–10 times that in the X-Z plane. The overall error amplitudes

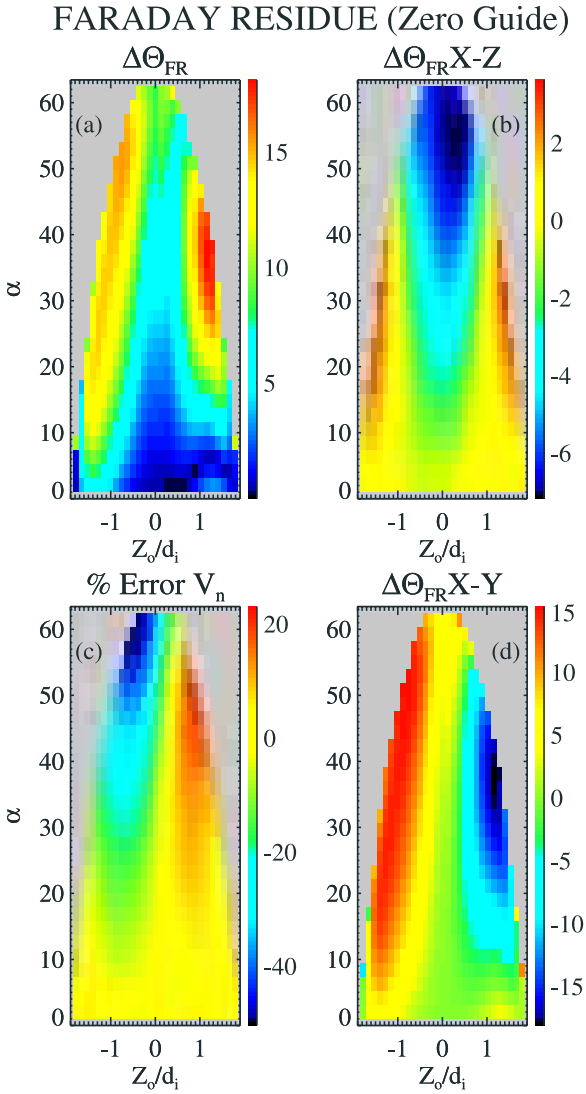

Figure 5. Overview of systematic errors MNVA(FR) for (a) normal recovery error, (b) normal error in x-z plane, (c) error in C_n, and (d) normal error along the x-y plane along the same world line trajectories as in Figure 2 for magnetopause layer with no guide field but two-dimensional structures. C_n = 15 km/s.

are significantly reduced versus MnVA(**B**). For any given crossing of the magnetopause layer, a single spacecraft's time series does not determine which W_{ij} pixel on the W chart pertains to the data under study. Thus the variability in the reconstruction exhibited here is a measure of the systematic uncertainty of inferring the normal to be in a particular direction as computed by MnVA(FR) for a specific time series. The strongly varying, world line-dependent natures of this uncertainty, makes it difficult to enhance the precision of the normal tighter than the worst error values in Figure 5. The relative speed of the structure inferred by this technique is neither high nor low relative to the correct value, although not symmetrically so.

3.4. MnVA(B) Versus MnVA(FR)

[30] A statistical picture of the scatter in Figures 2 and 5 is organized in different ways in Figure 6. Figure 6 (top) provides information on the accuracy of the derived normal when MnVA(**B**) and MnVA(FR) are both determined for the same world line. The horizontal axis is the angle in degrees between such inferred normals, while the ordinate is the lesser angular error to the true normal by either of the techniques. Arguments are made in the literature [e.g., *Mozer et al.*, 2002] that if the normals from MnVA(**B**)

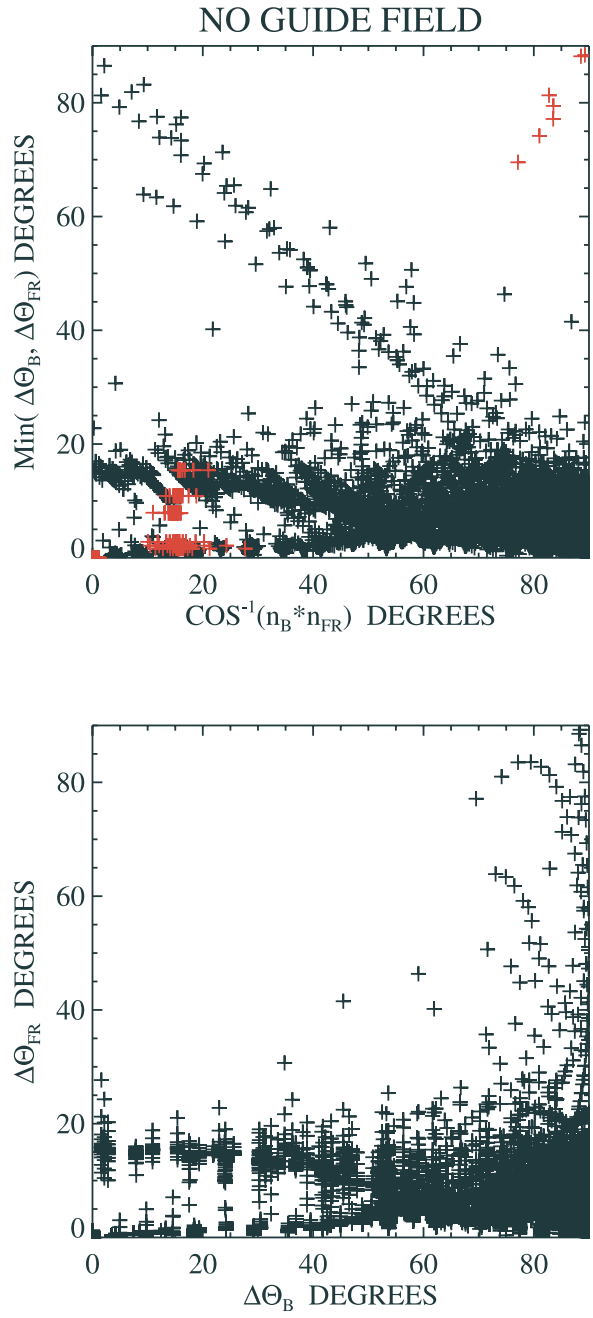

Figure 6. (top) No guide field. (bottom) Correlation of quality of normal recovery from MnVA(**B**) on the x axis versus same quantity from MnVA(FR): $\Delta\Theta_B$ versus $\Delta\Theta_{FR}$. In Figure 6 (top), symbols in red indicate the rare occurrences when the MnVA(**B**) normal is more nearly the correct normal than that from MnVA(FR). Ordinate is always better error estimate to the true normal. Abscissa is the angle between the MnVA(**B**) and MnVA(FR) normals.

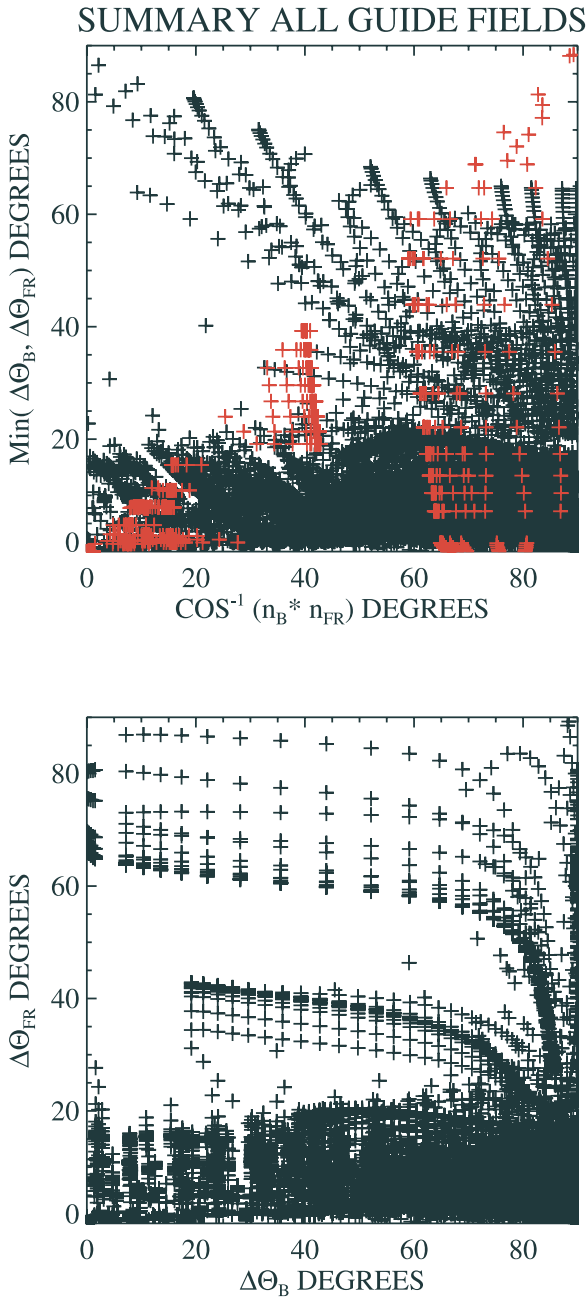

Figure 7. All guide fields. (top) Correlation of Minimum error to true normal with angle between MnVA(**B**) and MnVA(FR) suggested normal. Symbols are plotted in red on rare occasions when the MnVA(**B**) normal is more nearly the correct normal than that from MnVA(FR). (bottom) Correlations of errors of MnVA(FR) with MnVA(**B**).

and MnVA(FR) are close to one another, that they must be "collectively" close to the true answer and their precision is like their angular separation. The scatter of normal determinations on different world lines in this Figure 6 (top) illustrate (1) that MnVA(**B**) and MnVA(FR) normals are most frequently well separated and (2) that even when agreeing they can simultaneously not point in the true normal direction. This second conclusion is supported by the points in Figure 6 with negative slope that approach the left axis. At the same time there are also world lines (near the origin of this plot) where both methods give the same answer and both are nearly correct. This picture does not give a probability that either possibility is realized, but it does demonstrate that the following argument should not be used: "Because normals derived by MnVA(**B**) are close to those of MnVA(FR), the true normal is reliably inferred to be in the vicinity of these two normals." A better argument would be to use MnVA(FR) as the more generally correct normal direction in almost all cases, but to then still proceed with that normal propagating a 1σ systematic error of order 20°–25° as illustrated in Figure 6. Carefully done this would also imply letting the direction associated with the intermediate eigenvector also move to continuously provide an orthonormal basis. These effects impact the inferred size of the guide field or the tangential electric field since this basis ambiguity allows projection from irrelevant directions that may be large (such as $\mathbf{B}_T$ and dominate the inferred size of these projections). This estimate of uncertainty derives only from the two-dimensional character of the layer; any miscalibrations amongst the three components of $\mathbf{B}'$ or $\mathbf{E}'$ will reduce the precision further. These plots also show that the determination of the normal from magnetic data alone can be fraught with imprecision of a systematic type including errors that are essentially without preference between 0°–90°.

[31] Figure 6 (bottom) illustrates the organization of errors of the normal via MnVA(FR) with those via MnVA(B) on the same data set. Different points in Figure 6 (bottom) correspond either to different (1) trajectories across or (2) relative speeds along the normal to the layer. The general trend is to find the $\Delta\Theta_{FR}$ usually small and less than 20° even as $\Delta\Theta_B$ ranges from 0° to −90°. This summary examines all the different ways a no guide field layer could be presented to an observer and illustrates that the normal via MnVA(FR) is generally superior, although not always flawlessly close to the true normal (particularly as $\Delta\Theta_B \simeq$ 70°–90°.

[32] The construction of Figure 6 considers all world lines and trajectories through the same current sheet that possesses no guide field. Using spacecraft measurements, the a priori size of a guide field is unknown; accordingly a variety of guide fields must be considered when deciding the precision of the normal. A fairer presentation of the ambiguity of the normal given that the world line and guide field size are unknown is illustrated in Figure 7. The same format is used here as in Figure 6 to illustrate the larger systematic error on MnVA(FR) required in this situation, and the ongoing occurrence of circumstances where the MnVA(**B**) and MnVA(FR) can agree with one another at small angular separations, even though neither of these estimates is really close to the true current sheet normal.

3.5. Overview of Systematic Versus Statistical Error Estimates Using MVA

[33] The angular errors determined from the same self consistent no guide field 2-D current layers using MnVA(**B**), MxVA($\mathbf{E}'$), MnVA(FR) techniques are contrasted in Figures 8a, 8b, and 8d. These systematic errors are expressed in units of the statistical error for each technique and world line $\Delta\Theta^{K-S}(i, j)$. For reference, the systematic error in degrees of the normal determined by

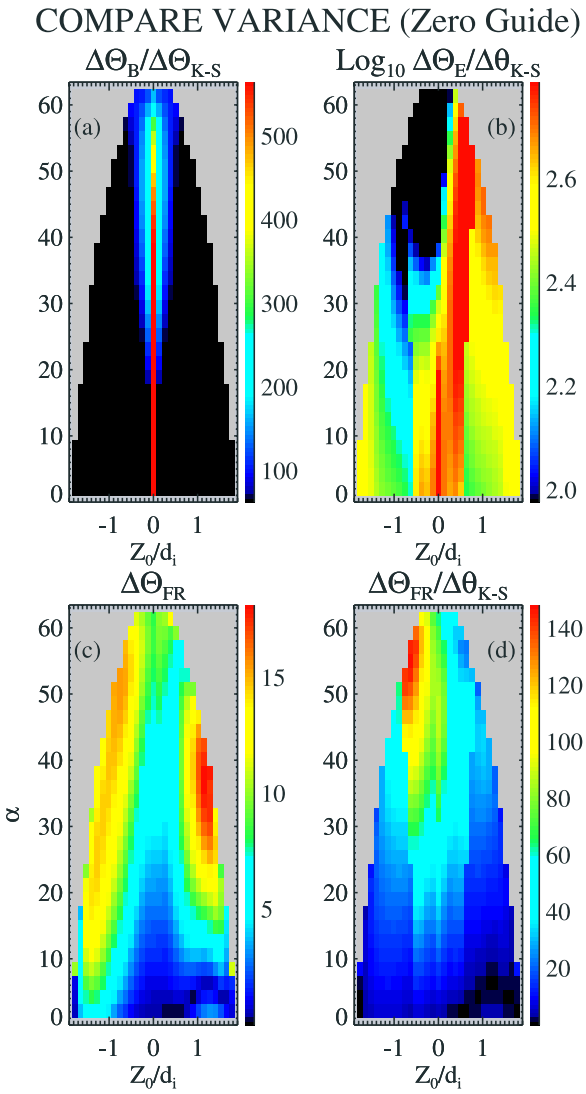

Figure 8. (a, b, and d) Systematic versus statistical error diagnostics on 2-D current sheet with no guide field. Observer is moving with C_n = 15 km/s. (c) Absolute size of systematic error in MnVA(FR) normal analysis in degrees.

MnVA(FR) is illustrated in Figure 8c. The systematic effects at the 2-D current sheets give rise to imprecisions $\Delta\Theta_B$ that can be more than 200 times (see Figure 8a) the sizes implied by the random error estimates of Sonnerup and Khrabrov for the data collected on these world lines. Almost without exception the systematic errors on MxVA(**E**′) exceed 200 times that by formal eigenvalue analysis. As expected the systematic errors of MnVA(FR) are not only smaller than the errors of the normal from MnVA(**B**), they are also generally smaller in units of the statistical errors (20–60 times the random errors on the basis of their eigenvalue separations; see Figure 8d). For those trajectories that pass near or through the separator MnVA(**B**) performs particularly poorly, while MnVA(FR) recovers the normal well in absolute terms. For the geometry inversion, these findings make a particularly strong case for making accurate, 3-D electric field measurements without proxies, and with all three components aliased over the same spatial scales in the plasma, so that MnVA(FR) can be routinely employed.

[34] The ensemble of errors at the magnetopause simulations surveyed in our study are assembled in the form of an expected error probability distribution (presuming no knowledge of world line) presented in Figures 9a and 9b for MVA(B) and MVA(FR) analyses separately. Figures 9a and 9b demonstrate that (1) rather routinely, MVA(**B**) does not provide a defensible normal, while (2) the less frequently used MVA(FR) can do so even in the presence of layers with two-dimensional substructure, provided the experi-

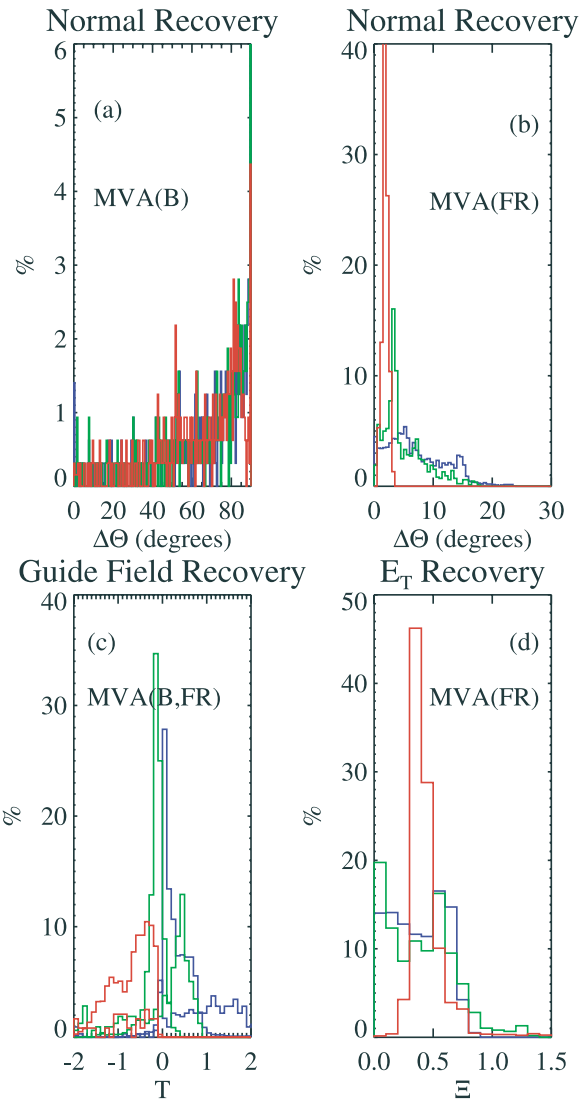

Figure 9. Overview of systematic errors in normals derived from (a) MnVA(**B**) and (b) MnVA(FR) along a spectrum of world lines, including variations in normal phase speed and considering layers of different guide field strength: blue, no; green, small; red, large. (c) Efficacy of guide field recovery, $\Delta\Upsilon$ via MnVA(**B**) (solid traces) and by MnVA(FR) (dashed traces), where guide field strengths are indicated by the same color codes as in Figures 9a and 9b. (d) Quality of recovery of the magnitude of the tangential electric field, $\Delta\Xi$, using MnVA(FR) normal and determined phase speed, C_n, again color coded for guide field strength.

mentalist propagates a rather large 1σ normal uncertainty of ~20° for no guide field layers through all computed results, including the implied imprecision of the adopted coordinate system influenced by the ambiguous normal. As the strength of the guide field grows to be comparable to the reconnecting component, the normal recovery of MnVA(FR) improves; this result presumably stems from the increased numerical importance and variability of the intercepted $B_y(t)$ profile. Figure 9c illustrates the distribution of $\Delta\Upsilon$, the departure of the inferred guide field from that in the simulation in units of the perceived variance of this component of **B** in the data. When a technique recovers the quantity on average, the mode of the histogram will be centered about zero. Having normalized the departures by the variance, "serious" discrepancies go with increasing absolute value of the modal values of the histogram. Figure 9d illustrates the quality, $\Delta\Xi$, of the recovery of the average modulus of the tangential electric field from that in the simulation. Zero $\Delta\Xi$ denotes a perfect recovery of the tangential electric field. These quantities involve projections of the electromagnetic field along directions determined by MnVA(**B**) and MnVA(FR) for all trajectories and all phase speeds as a color-coded function of size of guide field present: (blue none; green small; red large). When present MnVA(FR) determinations are illustrated with dashed segments, while those of MVA(**B**) are solid traces. Curves with the same color indicate sampling of model layers with the same imposed guide field.

[35] By construction the guide field for blue curves of the model solution is zero. Since the guide field itself is the average of a projection of **B** along the intermediate eigenvector's direction, this quantity is expected (by our results above for MnVA(**B**)) to be rather volatile, especially when it is noted that the direction of maximum variance is essentially fixed, but the direction of minimum variance is usually poorly determined (see Figure 9a). The mode of the blue solid histogram in Figure 9c is well removed from 0, indicating that the guide field estimates from MnVA(**B**) coordinate assignments will not usually be accurate, and erroneously suggest that a guide field has been inferred for the no guide (blue) model. For other guide field strengths MnVA(**B**) is not particularly persuasive, since the variance along this direction is enhanced due to the Hall variability in that direction. By contrast the guide field recovery with the MnVA(FR) coordinate system (indicated by the dashed histograms in Figure 9c) is notably more accurate, usually determining the guide field correct regardless of guide field strength. The dashed green histogram is nearly centered about zero, indicative of an on average recovery. Notwithstanding this improvement in performance the MnVA(FR) approach still suggests a sizable wing on the distribution even for the magnetopause layer with no guide field present. Hence extreme caution must be used when inventorying the evidence for a guide field from the adopted boundary normal coordinate picture of the layer, even if the normal and frame transformation was obtained by MnVA(FR).

[36] Since the MnVA(**B**) approach does not determine the front speed of the current layer, it cannot infer the conserved size of $\mathbf{E}_T$. A benefit of the MnVA(FR) method is that an estimate can be made of the rest frame tangential electric field. Figure 9d illustrates that with MnVA(FR) the recovery of this quantity is often in error on the order of the variance on the magnitude of the tangential electric field across the layer. For any given estimate of $\mathbf{E}_T$, its precision with MnVA(FR) is of the order of $\frac{1}{2}\sigma_{E_T}$.

3.6. Eigenvalue Ratio λ_2/λ_1 as Index of Errors in 2-D Layers

[37] There exist in the MVA literature various suggestions for culling "good" and "bad" normal determinations based on the spread of the intermediate, λ_2 to smallest, λ_1, eigenvalue of the MVA [*Siscoe et al.*, 1968; *Lepping and Behannon*, 1980]. While some authors accept a normal when $\lambda_2/\lambda_1 > 2$, the most recent review of this subject suggests this ratio should exceed 10 to be assured of detecting an accurate normal [*Sonnerup and Scheible*, 1998]. Some of this variation of opinion may stem from the range of realism of the models examined in the early simulations that did not include self consistent variations of the physical variables through the discontinuity [*Lepping and Behannon*, 1980] or had such coarse time resolution that 2-D layer substructures were almost never involved in the minimum variation process [*Siscoe et al.*, 1968].

[38] Reverting to the moment of inertia analogy of the covariance matrix discussed in Appendix A, disparate eigenvalues imply their associated eigenvectors are well-defined directions for simple rotation of the distributed mass. With real complications of time series, a related question to eigenvalue separation is the susceptibility of such a ratio to modifications by the various noise processes that accompany the data acquisition process itself. Clearly there is no general answer to this problem, unless there is a complete understanding of the sources of aberrant information in the time series that goes under the general sense of "noise" whether it is random or not. The discussion of this paper is about the role of 2-D variations in data sets being processed as if they were 1-D structures. In the general sense the 2-D structure embedded in the sampled time series represents highly correlated variations on the three components of $\mathbf{B}'$, $\mathbf{E}'$ superposed on the closest related 1-D electromagnetic structure. This "noise" need not be random, especially if it is being orchestrated by time-independent PDEs of the layer's possible reconnection electrodynamics. Using our moment of inertia problem for ease of visualization, these 2-D effects are like sprinkling mass on a body with well defined principal axes of inertia (well-separated λ values) and hoping that the new eigenvectors will not be reoriented after the new mass has been added to the body. The eigenvalue ratios available from the data processing are like those of the perturbed moment of inertia distribution; inverting from those directions the original mass distribution is difficult. Here too, we illustrate with our forward problem that diagnosing the importance of 2-D pollution in any given normal determination is not helped by studying the entrails of the eigenvalue ratios that are realized.

[39] We consider in Figure 10 all the world lines surveyed in our three simulations of the magnetopause with no, weak and strong guide fields; each row refers to a different guide field strength magnetopause model. Syntheses of eigenvalue analysis from MnVA(FR) determine the Figures 10a–10c, while those from MnVA(**B**) determine Figures 10d–10f. The ordinate of each plot is the absolute systematic error of normal recovery determined by this paper, while the

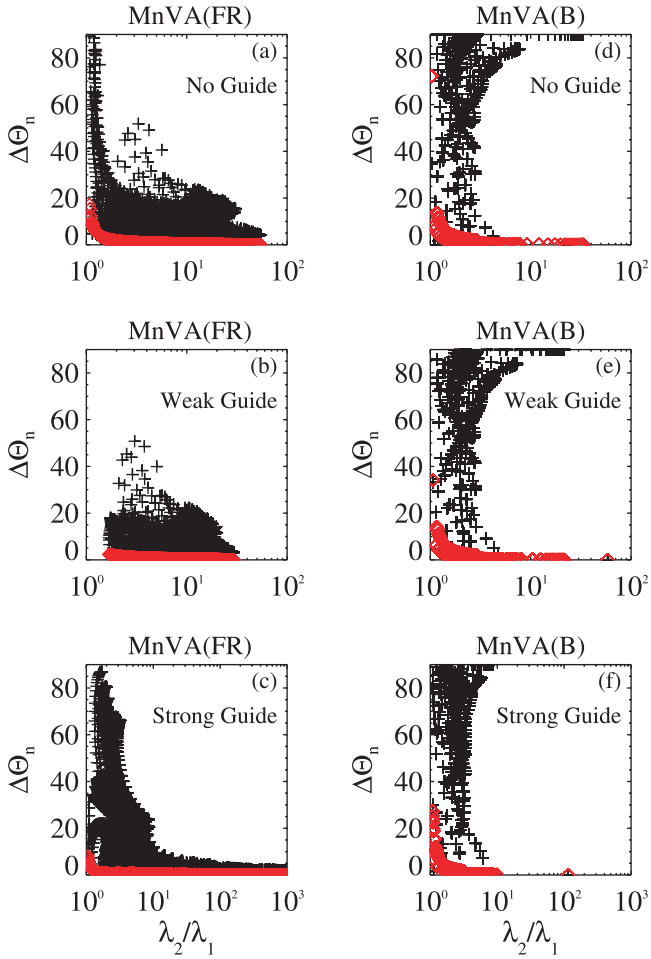

Figure 10. (a–c) Error of the normal direction determined via MnVA(FR) only as a function of λ_2/λ_1 and the evolution of such patterns with guide field strength. Each plot contains all world lines sampled for that guide field with that diagnostic technique. (d–f) Same diagnosis of the same layers, but now using MnVA(**B**). Because MnVA(**B**) does not have C_n sensitivity, there are fewer distinct symbols, while this dependence spreads out such readings in the upper row of MnVA(FR) analysis. The red diamonds are the locus of errors suggested for these data sets using the statistical methods of *Khrabrov and Sonnerup* [1998].

abscissa is the eigenvalue ratio λ_2/λ_1. Each cross plotted is the synthesis of a different MnVA determination along a different world line. The incidence of $\lambda_2/\lambda_1 > 10$ is only achieved with MnVA(FR) analysis on a subset of world lines; such eigenvalue ratios for MnVA(**B**) at the magnetopause for this data set are nonexistent. The occurrence of small normal errors (<20°) by MnVA(FR) is strongly organized by the enhanced eigenvalue ratio; conversely, very bad normal recovery by MnVA(FR) is strongly associated with $\lambda_2/\lambda_1 \leq 2-4$, with the lowest threshold for the no guide field simulation. Since most simulated and (actual) world lines for MnVA(**B**) analysis yield $\lambda_2/\lambda_1 \leq 4$, it is not surprising that their normal recovery is also uniformly poor. In passing, it should be noted that when interpretations have relied on inferred geometries at current layers, eigenvalue ratios $\lambda_2/\lambda_1 > 2$ may have been retained to have examples for further categorization. Such studies may need to be revisited since the present comparisons with the known normals of the simulations suggest that such normals and geometry were retained essentially out of exasperation, rather than any assurance that the directions inferred were of high precision.

[40] With the advent of direct measurements of all three components of $\mathbf{E}'$ on electrodynamics missions such as Polar or MMS, the use of MnVA(FR) should allow a more routine inversion of more precise geometry on any given event. From this study it is the one spacecraft technique of preference (short of a fuller Rankine Hugoniot MnVA), although it still has its intrinsic limitations in the presence of two-dimensional structures.

4. MVA of a Resolved, Oblique, 2-D Supercritical Shock Layer

[41] In the magnetopause layers studied above the two-dimensional subtext of the layer is a large-scale feature of the layer, with separatrices separated to frame a magneto-hydrodynamic exhaust which must be present in any steady state reconnection picture. If this analysis were repeated with at least a hybrid code's resolution of ion gyroscale phenomena, additional sources of higher dimensionality would also influence the normals. An example of such structures is revealed in the current layer of a supercritical shock which we now illustrate with the help of a hybrid solution. The analysis of a supercritical $M_A = 8$, oblique ($\theta_{Bn} = 65°$), $\beta_e = \beta_i = 0.5$ shock layer is presented in Figure 11. The speed of light in units of the Alfven speed is 6000. Figure 11a shows the systematic error of the MnVA(**B**) normal from the true normal as a function of where the world line pierces the layer (labeled Z_o/d_i) and the angle α of the world line as measured from the normal. This overview has been determined along world lines with C_n = 15 km/s. Since **B** is Galilean invariant, the MnVA(**B**) overview in (A) is typical of other values of C_n. Figure 11a reveals the uneven precision for recovery of the normal with MnVA(**B**). There are localized, but large, errors in the normal recovery (orange-red >70°) indicated in Figure 11a. These places have been highlighted in Figure 11a with a superposed diamond. The world lines that yield especially poor normal recovery of Figure 11a are indicated with black lines in Figures 11b and 11c superposed on the spatial variation of $|\mathbf{B}(x, z)|$ and $B_x(x, z)$, respectively. Along these unusual world lines the MnVA(**B**) procedure infers that the current sheet normal is well removed from the x direction, the true simulation normal, because the recorded variation of B_x has a significant variance along the path (see Figure 11). From our 2-D perspective and Figure 11c this variance is understandable.

[42] Within the 1-D premise of MnVA we also understand how the method picks another direction away from the true normal so that the variance of the observed $B_x(t)$ will be deemphasized. As an example, if the perceived variance in $B_x(t)$ is large, shifting the reported normal to an oblique angle to the coplanarity plane would reduce the perceived variation along that direction. Unlike the magnetopause simulations the large values of $\Delta\Theta_B > 45°$, occur in disorganized "clumps" in Figure 11a. Physically, these "error clumps" occur when world lines penetrate structures

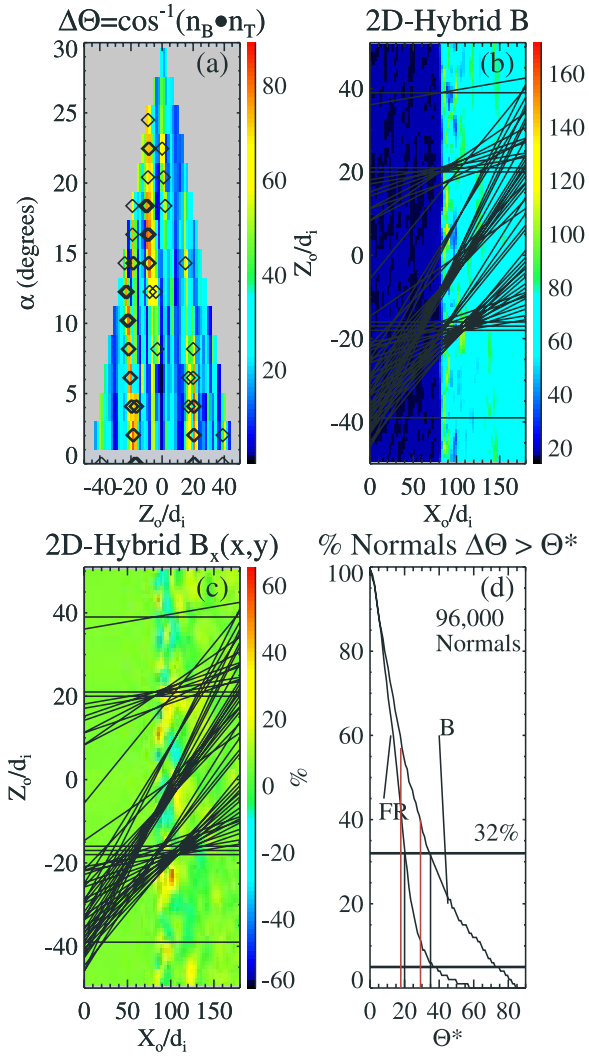

Figure 11. Summary of MVA diagnosis and errors at 2-D oblique supercritical shock using MnVA(**B**) and MnVA(FR). (a) MnVA(**B**) error of normal recovery as a function of angle of world line to the normal and position in second dimension of current sheet traversal. (b) Color-coded 2-D map of a snapshot of the magnetic intensity, $B(x, z, t_o)$. (c) Color-coded map of the component of **B** along the simulation's normal direction, $B_x(x, z, t_o)$. (d) Cumulative percentage distributions for MVA normal errors to exceed Θ*, segregated by MnVA(**B**) and MnVA(FR) techniques. C_n = 15 km/s. Black lines in Figures 11b and 11c indicate world lines identified in Figure 11a, where large errors or normal recovery are indicated. Such trajectories pass through major samples of z variations not contained in the MVA one-dimensional model.

in the magnetic overshoot controlled by finite Larmor radius effects of the ions. Figure 1 illustrates that these FLR structures provide a natural two-dimensional structuring to the shock layer that was not retained in the fluid models used above for the magnetopause current layer. Figure 11b color codes the magnetic field strength. Figures 11b and 11c emphasize the localized transverse "lumpy" scales of this problem, similar to those more regular variants in Figure 1b. The 2-D shock layer contains irregularly spaced 2-D "defects" that induce zones of high and low error for data collected along worldliness with specific intercept and slopes.

[43] Figure 11d is a statistical summary of the normal recovery of all MnVA(**B**) and MnVA(FR) variance computations done on the hybrid shock solution, including all different world lines and relative speeds of observer (which do impact the Faraday residue techniques for getting the normal and relative velocity when they get the normal). The ordinate is the percentage chance that the systematic error in the normal by MnVA(**B**) or MnVA(FR) is greater than the angular figure of merit on the horizontal axis, Θ*. The thick horizontal bar is the 32% line. These curves imply that the 1σ estimate for systematic error on the normal recovery is ~35° for MnVA(B) or ~20° for MnVA(FR). The vertical red lines are at the average positions of the distributions of errors. Thus, in the absence of any knowledge about the 2-D character or world line path through the shock, average MnVA(**B**) systematic error is 28°; minimum variance via FR is an overdetermined system with one more constraint ($\mathbf{E}_T$ = C) than MnVA(**B**) alone, and is a bit more robust with a 1σ error width of 17.5°. These error estimates are very idealized and the FR precision require three-axis $\mathbf{E}'$ measurements (which are not always available). It is clear now, why researchers often have used model shock normals for case and statistical studies when there is insufficient data to perform Rankine-Hugoniot geometry determinations [*Cairns et al.*, 1997; *Sigsbee et al.*, 2004].

[44] Comparison of Figures 11d and 9a illustrates the improvement in shocks of the MnVA(**B**) normal recover probability. The magnetopause layer normal recovery by MnVA(**B**) is essentially flat in the error angle to the true normal, whereas the shock distribution, while broader than MnVA(FR)s, is still strongly peaked about the average shock normal direction. This asymmetry would appear to be the result of the requirement that the extremes of the shock layer must satisfy the coplanarity theorem; the magnetic field within the actual shock layer does not satisfy the coplanarity theorem [*Goodrich and Scudder*, 1984; *Scudder*, 1995], determining a coherent variance in the components of **B** perpendicular to the coplanarity plane, partially dissuading the MnVA(**B**) technique from choosing it as the minimum variance direction. Notwithstanding this skew against the normal migration, the error on any given world line, cannot be reasonably expected to be less than 28°–30°. Even higher errors can occur as indicated in Figures 11a–11c; such realism implies that high reliability (95%) confidence error cone for a shock normal using MnVA(**B**) would widen to 75°. Multiple spacecraft passing through the shock layer, could determine the stationarity of the profile, to suggest how anomalous a given world line's sample of the overshoot might be. Alternatively, the overshoots of supercritical shocks could be edited out of the layer; however, to completely remove the layer leaves the method open to two nearly equally good MnVA(**B**) directions: that along the normal and perpendicular to the coplanarity plane. Such editing would leave MnVA(**B**) crippled by near or actual eigenvalue degeneracy, resulting in worthless normals indiscriminantly chosen in the plane perpendicular to

the maximum variance direction. An alternate route for this regime of eigenvalues has been explored recently [*Scudder*, 2005].

5. Why the Sensitivity?

[45] Part of the sensitivity of the minimum variance determination of normals can be traced to a well-known theorem about the roots of polynomials. They need not necessarily depend continuously on the variation of the coefficients [*Wilkinson*, 1959; *Acton*, 1990]. The eigenvectors of the variance matrix are each associated with the roots of the cubic characteristic polynomial of the variance matrix. As the world lines through the same time-independent structure smoothly change direction and/or speed there is no assurance that the eigenvectors associated with the inferred direction of minimum variance will always point in the same physical direction, nor evolve slowly in response to this slow variation in the coefficients of the eigenvalues characteristic polynomial. Examples of this sensitivity are illustrated by *Sonnerup and Scheible* [1998], where removing one data point caused the direction of minimum variance to rotate by 90°. As also discussed by Sonnerup, when the smallest and middle eigenvalue become comparable, the decision of the minimum eigenvalue and hence eigenvector is a computational tossup with implications that a vector 90° away from the minimum variance can be apparently chosen through round off errors.

[46] In addition to the capricious numerical issues associated with the eigenvalue problem that are well known, our present survey assays the impact on the recovery of the current sheet normal of systematic and correlated variations of all three components of **E** and **B** in the time series witnessed by an observer moving through a layer containing variations transverse to the normal. While Maxwell always requires $\nabla \cdot \mathbf{B} = \mathbf{0}$, it is no longer generally true in our 2-D layers that this equation is satisfied by a constant component along the normal. Thus, while the minimum variance direction may still be found, it has in this situation no a priori theoretical connection to the direction of the true normal of the current sheet. Such realistic and self-consistent layers contain features that are outside the model premises of MVA. These two-dimensional effects are embedded in the variance matrix no matter what vector time series it works on. Figure 2a indicates that this systematic imprecision can commonly be in excess of 20° and often will be larger. With four physical examples we have illustrated circumstances where the MVA normal will depend on the precise coordinate where the world line passes through the current sheet. It should be noted that even when the relative phase speed along the current sheet normal is determined, there remains insufficient information to reconstruct the observer's world line through the layer. Together with the unknown size of the guide field present in the layer, any given current sheet analysis has at least three hidden variables which this study has illustrated can affect estimates of the systematic errors of the normal: these are (1) the total relative velocity, (2) the precise location of the world line's traversal of the current sheet, and (3) the size of the guide field itself. Until multiple spacecraft techniques are perfected to remove some or all of these ambiguities, the systematic error on a current sheet normal determination can hardly be construed as better than 25° to the inferred direction from MnVA(FR) when applied to measured 3-D electric and magnetic field time series.

6. Summary

[47] We have examined the world line dependence of MVA inferences of current sheet normals for a hybrid oblique supercritical shock layer and Hall MHD simulations of magnetopause layers with no, weak and strong guide fields. We have demonstrated that the MVA can have strong systematic errors that enlarge their systematic uncertainties relative to those determined by the usual eigenvalue error analysis. We have shown that MnVA(FR) is more robust (but not error free) at determining the geometry at the magnetopause than MnVA(**B**); at the shock layer MnVA(FR) is still superior, compared to MnVA(**B**). We have demonstrated that MxVA($\mathbf{E}'$) at layers with strong magnetic shear such as the magnetopause or bow shock are virtually without value, unless the transformation speed to the current layer frame is known elsewhere, (which is equivalent to solving MnVA(FR), so the critique of MxVA($\mathbf{E}'$) remains. We have also shown that for the simulations undertaken in this study that intermediate to smallest eigenvalues for MnVA less than 2–4 accompany particularly poor normal determinations and when either MnVA(**B**) or MnVA(FR) yield eigenvalue ratios, $\lambda_2/\lambda_1 > 10$ that their 2-D systematic errors are minimized. We have also emphasized that our evaluation of MnVA(FR) was made while using $\mathbf{B}'$ and $\mathbf{E}'$ as fully measured vectors (rather than proxies for $\mathbf{E}'$, or spin plane components of $\mathbf{E}'$ together with $\mathbf{E} \cdot \mathbf{B} = 0$ as has been done in the past). In this sense the rough rule of thumb developed here about the angular precision of the normal from MnVA(FR) must be considered a floor for the actual errors involved when $\mathbf{E}' \cdot \mathbf{B}' = 0$ is enforced or $\mathbf{E}' = -\mathbf{U}' \times \mathbf{B}'$ proxies are used to compensate for unmeasured components of or the entire vector $\mathbf{E}'$.

[48] Finally, it should be emphasized that MnVA(**B**), MnVA(FR) are part of a subset of tests based on conservation laws of conducting magnetized fluids that obtain geometry by finding Galilean shifts and coordinate rotations so that the Maxwell/Fluid equations and Rankine-Hugoniot conservation laws are optimally satisfied at time stationary layers that are assumed to be one-dimensional. Of this subset MnVA(**B**) is the weakest since it involves only one conservation law. MnVA(FR) is more robust, involving two conservation laws. Formulations exist for picking the geometry and speed of 1-D discontinuities from time series using more conservation laws and more observables along the same time series [e.g., *Viñas and Scudder*, 1986] to improve the overdetermination of the key observables of average normal and relative speed. In the comparisons presented here the technique with more constraints (MnVA(FR)) yields lower errors and more routine retrieval of the normal, even in the presence of 2-D effects. The new conservation laws that add additional constraints, such as normal mass flux, tangential momentum flux conservation, and beyond should, in principle, yield more overdetermined equations for the same world line, and should yield a better average normal with fewer distractions from the almost

unavoidable two-dimensional effects that defeat fewer and simpler tests.

Appendix A

[49] All MVA techniques (or phase front techniques using multispacecraft) suppose the current layers are locally planar and stationary in the frame of reference where the current layer is at rest. This assumption formally allows the determination of an orthonormal basis by MVA in which the minimum variance direction is usually taken to be the local surface normal. In passing it should be noted that MnVA(**B**) [*Sonnerup and Cahill*, 1968] and MnVA(FR) [*Khrabrov and Sonnerup*, 1998] are specializations of MVA associated with conserving the Rankine-Hugoniot equations across discontinuities in continuum electrodynamics [*Viñas and Scudder*, 1986]. As a practical matter these variance techniques compare various components of the same vector time series, (MnVA(**B**), or compare functions of components of two or more vector fields, (MnVA(FR) or Rankine-Hugoniot itself). It can often be the case that all three components of the same vector field do not have the same precision, and it is most certainly the case that the determinations of $\mathbf{E}'$ and $\mathbf{B}'$ do not have either the same magnitude or directional precision. Accordingly the minimum variance procedures with real data must inform the theoretically motivated minimization techniques what variations are of significance and those that are not. To date this has usually not been the practice and may be a factor in the quality of information that is extracted from such analyses. Further, the third (spin) axis of E' when measured directly is usually bolstered, if not defined, by imposing the assumption that $\mathbf{E}' \cdot \mathbf{B}' = 0$, a relation that is generally not expected to be true in current layers. The central premise of these variance techniques beyond the 1-D approximation is that the vector fields in use are characterizing the same volume of plasma. A subtle issue of a similar type would occur when using two of the components of **E** from spin plane wires and determining the spin axis electric field with a much shorter boom or an electron drift determination [*Paschmann et al.*, 1998]. If the spin plane wires sense potential differences over scales large compared to the Debye shielding lengths for the photoelectron cloud about the spacecraft, while the on axis boom retains some signal from the surrounding sheath of the spacecraft and some ambient information, the triad, $\mathbf{E}'$ is unsuitable for MnVA. If the vector $\mathbf{E}'$ is assembled from different techniques all three components should not be treated on an equal footing in these MVA analyses. Examples of such compromises are the use of a returned electron beam to measure one or more components of **E** while relying on boom measurements for other components. The drift technique returns information about the gyroaveraged component of **E** that is a spatial average over the beam electrons gyro path which in general can be much different that the boom lengths for the remaining components. While the spacecraft moves the boom sampled E components are also spatial averages as well, but over spatial scales that are much smaller than the gyroscale.

[50] Variance techniques always return answers; this robustness must be tempered by an evaluation (1) that the analyzed raw vector fields have components that are truly compatible in the sense discussed above; (2) that the minimization procedure is aware, before selecting the eigenvectors, of the measurement uncertainties of all components of all vector fields used in the analysis; and (3) that the inverse information so robustly calculated has a robust association with being an accurate representation of the underlying geometry of the current layer. We are aware of five attempts to reformulate the minimization problems that attempt to balance the known measurement issues en route to the normal determination [*Lepping and Argentiero*, 1971; *Acuña and Lepping*, 1984; *Viñas and Scudder*, 1986; *Lindqvist and Mozer*, 1990; *Scudder et al.*, 1999].

[51] By contrast in this paper we are dealing with electrodynamic variables determined by the numerical solution of partial differential equations using fourth-order accurate methods which determine **E** and **B** at comparable precision, so that (1, 2) above are not involved in our survey. By design our focus is concern (3). We thus use the standard MnVA(**B**) and MnVA(FR) techniques for our examination of the systematic errors involved in this paper. The inaccuracies reported here represent lower bounds to the general sources of imprecision the experimentalist faces since they correspond to perfectly calibrated data with no systematic or unmatched calibration errors of **B** and **E** or the latter's proxies.

[52] In the case of MnVA(**B**), Gauss's law under the 1-D spatial premise is used to suggest that there is a preferred direction, $\hat{\mathbf{n}}$, along which the projection of the magnetic field, B_n, has the minimum dispersion compared to any other direction on the unit sphere. The central assumptions of this approach are (1) $\nabla \cdot \mathbf{B} \equiv \dfrac{\partial B_n}{\partial n}$, and (2) that the causes for time variations **B** detected in the spacecraft frame are only those induced by convection of a one-dimensional spatial structure that is otherwise actually time-independent in its rest frame. Intrinsic time variations in the structure that may be superposed on the spatial structure will modify the derived direction of minimum variance determined from such data in an unknown way.

[53] The MnVA(FR) technique seeks to exploit the special time and space variation of a phase standing one-dimensional structure in all frames: without loss of generality such a quantity must be a function of time and space only through the bilinear combination of $\chi = n - C_n t$, where n is the spatial coordinate along that only direction where spatial variation is assumed to exist, and C_n is the unknown relative speed of the structure along its normal as determined in the observer's coordinates, and t is the observer's time. This bilinear functional form is motivated by the method of characteristics; Galilean relativity provides the identification of C_n as the phase front's speed (reckoned in the spacecraft frame). The bilinear form leads to the simplification of Faraday's Law from a partial differential equation to a separable, and thus integrable, ordinary differential equation relating total differentials of **B** and the parts of $\mathbf{E}'$ transverse to the unknown normal [*Khrabrov and Sonnerup*, 1998]. An immediate vector integration constant of this ODE is $\Gamma' = C_n \mathbf{B}'/c - \mathbf{n} \times \mathbf{E}'$ which is a different vector constant for each observer of the layer recording $\mathbf{E}'$, $\mathbf{B}'$ along world lines with different C_n. For an observer at rest in the frame of the discontinuity Γ_R is the rest frame tangential electric field. Gauss's law is also used in this formulation, so that MnVA(FR) represents

a superset of constraining equations relative to MnVA($\mathbf{B}$), while still itself remaining as a proper subset of the Hugoniot conservation conditions across the front. The MnVA(FR) technique determines a phase speed, C_n and assigns the normal direction and by this the three components of the conserved vector Γ' so that its Pythagorean variance is a minimum [*Terasawa et al.*, 1996]. Like the general Hugoniot problem [*Viñas and Scudder*, 1986] the Faraday residue technique is a "mixed" technique requiring information from different measurement variables and hence errors. Clearly the derived quantities phase speed and normal vector depend on the error signals that remain in the vector coordinates used in the subsequent analysis. Such experimental errors, while present in any real data set, are not considered here.

[54] MxVA($\mathbf{E}'$) has occasionally been used to infer normals [*Paschmann et al.*, 1986; *Sonnerup et al.*, 1987; *Sonnerup et al.*, 1990; *Hull et al.*, 2003]. The motivation of this technique is that the tangential electric field in the rest frame of the assumed one-dimensional current structures should be constant. In the rest frame of the current the only variance of $\mathbf{E}$ expected would be preferentially along the local normal of the current layer. However, the available (or proxy) electric field, $\mathbf{E}'(t)$, is recorded in the time domain on a spacecraft moving with respect to the layer; if it were not so the observer would not traverse the layer. Since $|\mathbf{E}'| \ll |\mathbf{B}'|$ this unknown relative motion makes an important Galilean correction to the rest frame electric field inventoried. These contributions affect the computed covariance of $\mathbf{E}'$, provided the direction of $\mathbf{B}$ is changing through the layer. When $\mathbf{B}$ has strong shear, as at a magnetosonic shock or at the magnetopause, this cross frame dependence is "undone" by MnVA(FR) as it attempts to correct for the relative phase velocity, transforming the observed $\mathbf{E}'$ back to the layer's rest frame $\mathbf{E}$ before enforcing conservation of tangential $\mathbf{E}$. An additional problem with proxy electric fields determined from the ions and the unipolar contribution, is that they are only asymptotically a measure of the electric field (in places where there is no current density or pressure gradients) and not generally an accurate measure of $\mathbf{E}'$ through the current carrying layer [*Scudder*, 1997; *Scudder et al.*, 1999]. For those layers where Hall signatures are not present [*Sonnerup et al.*, 1987] have argued that unipolar approximations to $\mathbf{E}'$ should be acceptable. These authors have also used a transformation of the proxy $\mathbf{E}'$ data to the deHoffmann-Teller frame to affect MxVA($\mathbf{E}^{HT}$). Strong electric fields seen in the auroral zone can occur across a very weakly sheared magnetic interface [*Hull et al.*, 2003]; while formally MnVA(FR) should always determine a better normal, MxVA($\mathbf{E}'$) results are acceptable in these small shear layers since the nonzero frame transformation correction to the observer's sense of the correlated variance of all the components of $\mathbf{E}'$ and is small in this circumstance.

[55] This paper comments on MVA determinations at layers where there is a perceptible magnetic shear as at tangential, rotational discontinuities or shock layers. For these layers the variance of the electric field is not even approximately Galilean invariant, and unmodified MxVA($\mathbf{E}'$) is totally without utility, since it is compromised by systematic defects associated with the motion of the spacecraft even were the layer precisely one-dimensional. If the layer contains two-dimensional features, the normals have additional distractions, since the motivational premise of MxVA($\mathbf{E}'$) is an inadequate attempt at MnVA(FR).

[56] In all cases of MVA the object of analysis is the 3×3 variance matrix, $\mathbb{C}$, its unit eigenvectors, ε_j, and eigenvalues, λ_j. $\mathbb{C}$, is computed from the time series of the vector $\mathbf{V}(t)$ through the layer as the positive definite 3×3 symmetric variance matrix,

$$\mathbb{C}_{ij}(\mathbf{V}) = \langle V_i V_j \rangle - \langle V_i \rangle \langle V_j \rangle$$

determined from the components of the vector field, $V_i(t_k)$ recorded at times $(t_1, t_2, .., t_n)$ through the layer. The angular brackets denote the arithmetic average of the quantity sampled over time. If we denote the individual components in terms of their average V_j and deviations, δv_j, $\mathbb{C}$ simplifies to become

$$\mathbb{C}_{ij}(\mathbf{V}) = \mathbb{C}_{ij}(\delta \mathbf{v}) \equiv \langle \delta v_i \delta v_j \rangle$$

An intuitive feel for the shaping factors of the variance matrix can be obtained by noting its many similarities with the more familiar moment of inertia matrix, I_{ij}, of mechanics. In terms of the separation $\delta\mathbf{r}(k)$ from the center of mass of k equal masses, I_{ij} is given by

$$I_{ij} = M\left(\delta_{ij}\langle|\delta\mathbf{r}(k)|^2\rangle - \mathbb{C}_{ij}(\delta\mathbf{r}(k))\right)$$

where M is the total mass of the discrete masses. The first term is the irreducible spherical assessment, S, of the dispersion of mass in I_{ij}, while the correction $\mathbb{C}_{ij}$ matrix signals the quadrupolar departures from sphericity of the mass distribution. When the first term is nonzero, the mass distribution can store energy isotropically in rotation about the center of mass. When the elements of $\mathbb{C}_{ij}$ are nonzero, the mass distribution is not spherical, and will have preferred orientations for simple rotation. The eigenvalues λ^S of the spherical portion of S are triply degenerate, having the common value $\lambda^S = M\Sigma_j\lambda_j$, where the λ_j are the eigenvalues of $\mathbb{C}$. Thus the eigenvalues of the moment of inertia matrix are $\lambda_k^I = \lambda^S - M\lambda_k$. These relations identify the spectrum of the eigenvalues of the variance matrix as controlling the existence of preferred axes of the moment of inertia ellipsoid. If all λ_j are computationally distinct there are three unique axes in space for simple angular motion. For completeness, it may be seen that the direction of maximum mass dispersion associated with MxVA($\delta\mathbf{r}$), actually yields, via subtraction, the minimum eigenvalue of the moment of inertia tensor. A cylindrical cigar shaped uniform density mass distribution possesses its maximum mass variance along the long axis of the cigar; accordingly, by this reasoning, this axis is the easiest about which to torque the cigar and, correctly, corresponds to the axis of the minimum eigenvalue of I_{ij}.

[57] Taking this analogy a bit further, one can inquire what would happen if more mass was added to the rigid body, but in such a way that the center of mass was not modified. In general such an addition would increase the variance along x, y, and z in a correlated way, that would change the eigenvalue structure and reorient the principal axes of the moment of inertia ellipsoid, determined by the eigenvalues of a perturbed I'_{ij}. Since the preferred directions

are determined by the quadrupolar correction terms, it is now clear that new sources of mass dispersion must be added either (1) equally to all three orthogonal axes, or (2) in fixed proportions that reflect the original mass dispersion to leave the eigendirections of the unperturbed I_{ij} unchanged. Insofar as MVA attacks problems outside of the intended 1-D layers, there will be correlated additional variances included in $\mathbb{C}_{ij}$ that reflect the 2-D character of the observed electromagnetic field through the layer. Rather special circumstances can be posited where the eigenvectors of $\mathbb{C}_{ij}$ remain unchanged, but they would appear unlikely to be realized in nature since the size of the variance of $\mathbf{B}'$ or $\mathbf{E}'$ along all three axes are not separately selectable, but orchestrated by the augmented MHD equations that define the structures being examined. This viewpoint also illustrates the challenge of various filtering strategies that have been suggested to remove "extraneous" sources of variance within the layers traversed.

[58] Comparing I_{ij} and $\mathbb{C}_{ij}$ we see that the analogue of displacement, $\delta\mathbf{r}(k)$, of individual equal masses from the center of mass is the departure, $\delta\mathbf{r}(k)$ at each time of the vector field, $\mathbf{V}$, from it average value, $\langle\mathbf{V}\rangle$. It should thus be anticipated that the rearrangement of any variation of components about their mean value, or repartition amongst the variances of the three components, or new sources of variance, will almost without exception, affect the preferred axes (eigenvectors) of the variance matrix in much the same way as the redistribution of matter about the center of mass will affect the orientation of the preferred axes of the moment of inertia ellipsoid. We illustrate in the text that the contrast of a 2-D layer with a 1-D layer is precisely to add new, and correlated, sources of variance in the sampled vector field, inducing a rearrangement of the eigenvectors.

[59] The matrix elements of I_{ij} and $\mathbb{C}_{ij}$ are both real, symmetric and, hence Hermitian with real eigenvalues. From such eigenvectors a right-handed orthonormal basis may always be constructed. The orientations of ε_j in space are determined from $\mathbb{C}_{ij}$ to within an arbitrary sign. In what follows we choose the sense of the minimum variance eigenvector ε_1 so that its x component is positive, the direction of the intermediate eigenvector, ε_2 is chosen to have its y component negative. The sense of the maximum variance direction, ε_3 is then determined by the right hand rule, generating a right handed orthonormal basis.

[60] If two eigenvalues of $\mathbb{C}_{ij}$ are actually degenerate the ε_k associated with them are not uniquely determined, with infinitely many pairings of eigenvectors possible. In this situation no peculiar direction can be determined in the plane perpendicular to the third, distinct, eigenvector. However, in this circumstance most eigenvalue-eigenvector routines supply eigenvectors without user intervention, usually by implementing Gram-Schmidt orthogonalization [e.g., *Arfken and Weber*, 2001]. Thus eigenvector analysis is robust in that it always gives an answer, but its relevance to the physical problem requires further screening based on the relative sizes of eigenvalues. Degenerate eigenvalues can occur even when the current layers are truly one-dimensional. The minimum or maximum variance direction of a 3×3 matrix must be a part of this degeneracy when it occurs. In the presence of such unresolved degeneracy the utility of the variance technique for determining quantities projected along the normal or transverse to it and the maximum variance direction are totally useless. The linearized error analysis for sensitivity to random error involves the difference of the eigenvalues; near eigenvalue degeneracies imply large error cones on the orientation of the associated eigenvectors. Operationally, the question of degree of degeneracy becomes how distinct is sufficient to proceed with a physical assignment of a meaningful direction. Data analysis that is stymied without a good normal often proceeds with quasi-degenerate solutions simply to proceed with publication, rather than acknowledging that the data will not support such an organization nor conclusions dependent on it. A new approach for such layers has recently been published [*Scudder*, 2005].

[61] When represented in their principal axes basis, $\mathbb{C}$ is diagonal, taking on the form

$$\mathbb{C}'_{ij} = \delta_{ij}\lambda_j; \lambda_j \geq 0$$

The minimum variance is equal to the minimum λ_j, which is in turn the projection of the variance matrix onto the minimum variance direction:

$$\mathbb{C}'_{11} \equiv \hat{\mathbf{n}} \cdot C \cdot \hat{\mathbf{n}} \equiv \lambda_1$$

[62] Using the eigenvectors of $\mathbb{C}$ as a new basis, the vectors of the original time series of $\mathbf{V}(t)$ can be rotated into this primed coordinate system, $\mathbf{V}'(t)$, announced in the literature without fanfare: "...transforming to boundary normal (minimum variance) coordinates...". Such a procedure is computationally deterministic and will always produce "a" minimum variance direction, $\hat{\mathbf{n}} \equiv \hat{\varepsilon}_1$ along which the root mean square variation of that component of $\mathbf{V}$ is minimal. The text of this paper illustrates that such rotations, while always possible, need not always be "the" physically desired coordinate system for the layer.

[63] **Acknowledgments.** Discussions with A. J. Hull, F. S. Mozer, N. C. Maynard, and D. Ober are acknowledged.

[64] Lou-Chuang Lee thanks the two reviewers for their assistance in evaluating this paper.

References

Acton, F. S. (1990), *Numerical Methods That Work*, Mathematical Association of America, Washington, D. C.

Acuña, M. H., and R. P. Lepping (1984), Modification to shock fitting program, *J. Geophys. Res.*, *89*(A12), 11,004–11,006.

Aggson, T. L., N. C. Maynard, and P. J. Gambardella (1983), Electric field measurements at the magnetopause: 1. Observation of large convective velocities at rotational magnetopause discontinuities, *J. Geophys. Res.*, *88*(A12), 10,000–10,010.

Arfken, G. B., and H. J. Weber (2001), *Mathematical Methods for Physicists*, Wiley-Interscience, Hoboken, N. J.

Cairns, I., P. A. Robinson, R. R. Anderson, and R. J. Strangeway (1997), Foreshock Langmuir waves for unusually constant solar wind conditions: Data and implications for foreshock structures, *J. Geophys. Res.*, *102*(A11), 24,249–24,264.

Goodrich, C. C., and J. D. Scudder (1984), The adiabatic energy change of plasma electrons and the frame dependence of the cross-shock potential at collisionless magnetosonic shock waves, *J. Geophys. Res.*, *89*(A8), 6654–6662.

Hau, L.-N., and B. U. Ö. Sonnerup (1999), Two-dimensional coherent structures in the magnetopause: Recovery of static equilibria from single-spacecraft data, *J. Geophys. Res.*, *104*(A4), 6899–6918.

Hudson, P. D. (1970), Discontinuities in an anisotropic plasma and their identification in the solar wind, *Planet. Space Sci.*, *18*(11), 1611–1622.

Hull, A. J., J. Bonnell, F. S. Mozer, and J. D. Scudder (2003), A statistical study of large-amplitude parallel electric fields in the upward current region of the auroral acceleration region, *J. Geophys. Res.*, *108*(A1), 1007, doi:10.1029/2001JA007540.

Khrabrov, A. V., and B. U. Ö. Sonnerup (1998), Orientation and motion of current layers: Minimization of the Faraday residue, *Geophys. Res. Lett.*, *25*(13), 2373–2376.

Lepping, R. P., and P. D. Argentiero (1971), Single spacecraft method of estimating shock normals, *J. Geophys. Res.*, *76*(19), 4349–4359.

Lepping, R. P., and K. W. Behannon (1980), Magnetic field directional discontinuities: 1. Minimum variance errors, *J. Geophys. Res.*, *85*(A19), 4695–4703.

Lindqvist, P.-A., and F. S. Mozer (1990), The average tangential electric field at the noon magnetopause, *J. Geophys. Res.*, *95*(A10), 17,137–17,144.

Ma, Z. W., and A. Bhattacharjee (1996), Fast impulsive reconnection and current sheet intensification due to electron pressure gradients in semi-collisional plasmas, *Geophys. Res. Lett.*, *23*(13), 1673–1676.

McKean, M. E., N. Omidi, D. Krauss-Varban, and H. Karamabadi (1995), Wave and particle evolution downstream of quasi-perpendicular shocks, *Adv. Space Res.*, *15*(8/9), 319–322.

Meziane, K., A. J. Hull, A. M. Hamza, and R. P. Lin (2002), On the bow shock Θ_{Bn} dependence of upstream 70 keV to 2 MeV ion fluxes, *J. Geophys. Res.*, *107*(A9), 1243, doi:10.1029/2001JA005012.

Mozer, F. S., S. Bale, and T. Phan (2002), Evidence of diffusion regions at a subsolar magnetopause crossing, *Phys. Rev. Lett.*, *89*(1), 015,002-1–015,002-4.

Paschmann, G., I. Papamastorakis, W. Baumjohann, N. Sckopke, C. W. Carlson, B. U. Ö. Sonnerup, and H. Lühr (1986), The magnetopause for large magnetic shear: AMPTE/IRM observations, *J. Geophys. Res.*, *91*(A10), 11,099–11,115.

Paschmann, G., C. E. McIlwain, J. M. Quinn, R. B. Torbert, and E. C. Whipple (1998), The electron drift technique for measuring electric and magnetic fields, in *Measurements Techniques in Space Plasmas: Fields*, *Geophys. Monogr. Ser.*, vol. 103, edited by R. Pfaff and J. Borovsky, pp. 29–38, AGU, Washington, D. C.

Scudder, J. D. (1995), A review of the physics of electron heating at collisionless shocks, *Adv. Space Res.*, *15*(8/9), 181–223.

Scudder, J. D. (1997), Theoretical approaches to the description of magnetic merging: The need for finite β_e, anisotropic ambipolar Hall MHD, *Space Sci. Rev.*, *80*, 235–267.

Scudder, J. D. (2005), Geometry of magnetosonic shocks and plane-polarized waves: Coplanarity Variance Analysis (CVA), *J. Geophys. Res.*, *110*, A02202, doi:10.1029/2004JA010660.

Scudder, J. D., A. Mangeney, C. Lacombe, C. C. Harvey, T. L. Aggson, R. R. Anderson, J. T. Gosling, G. Paschmann, and C. T. Russell (1986), The resolved layer of a collisionless high β, supercritical, quasi-perpendicular shock wave: 1: Rankine-Hugoniot geometry, currents, and stationarity, *J. Geophys. Res.*, *91*(A10), 11,019–11,052.

Scudder, J. D., P. A. Puhl-Quinn, F. S. Mozer, K. W. Ogilvie, and C. T. Russell (1999), Generalized Walén tests through Alfvén waves and rotational discontinuities using electron flow velocities, *J. Geophys. Res.*, *104*(A9), 19,817–19,833.

Sigsbee, K., C. A. Kletzing, D. A. Gurnett, J. S. Pickett, A. Balogh, and E. Lucek (2004), The dependence of Langmuir wave amplitudes on position in Earth's foreshock, *Geophys. Res. Lett.*, *31*, L07805, doi:10.1029/2004GL019413.

Siscoe, G. L., L. Davis Jr., P. J. Coleman Jr., E. J. Smith, and D. E. Jones (1968), Power spectra and discontinuities in the interplanetary magnetic field: Mariner 4, *J. Geophys. Res.*, *73*(1), 61–82.

Sonnerup, B. U. Ö., and L. J. Cahill Jr. (1968), Explorer 12 observations of the magnetopause current layer, *J. Geophys. Res.*, *73*(5), 1757–1770.

Sonnerup, B. U. Ö., and M. Scheible (1998), Minimum and maximum variance analysis, in *Analysis Methods for Multi-Spacecraft Data*, pp. 185–220, Springer, New York.

Sonnerup, B. U. Ö., I. Papamastorakis, G. Paschmann, and H. Lühr (1987), Magnetopause properties from AMPTE/IRM observations of the convection electric field: Method development, *J. Geophys. Res.*, *92*(A11), 12,137–12,159.

Sonnerup, B. U. Ö., I. Papamastorakis, G. Paschmann, and H. Lühr (1990), The magnetopause for large magnetic shear: Analysis of convection electric fields from AMPTE/IRM, *J. Geophys. Res.*, *95*(A7), 10,541–10,557.

Sonnerup, B. U. Ö., S. Haaland, G. Paschmann, B. Lavraud, M. W. Dunlop, H. Rème, and A. Balogh (2004), Orientation and motion of a discontinuity from single-spacecraft measurements of plasma velocity and density: Minimum mass flux residue, *J. Geophys. Res.*, *109*, A03221, doi:10.1029/2003JA010230.

Terasawa, T., H. Kawano, I. Shinohara, T. Mukai, Y. Saito, M. Hoshino, S. Machida, T. Nagai, and T. Yamamoto (1996), On the determination of a moving MHD structure: Minimization of the residue of integrated Faraday's equation, *J. Geomagn. Geoelectr.*, *48*, 603–614.

Viñas, A. F., and J. D. Scudder (1986), Fast and optimal solution to the Rankine-Hugoniot Problem, *J. Geophys. Res.*, *91*(A1), 39–58.

Wilkinson, J. H. (1959), The evaluation of the zeroes of ill-conditioned polynomials, part 1, *Numer. Math.*, *1*, 150–166.

Z.-W. Ma and J. D. Scudder, Department of Physics and Astronomy, University of Iowa, Iowa City, IA 52242, USA. (jack-scudder@uiowa.edu)

N. Omidi, Department of Electrical Engineering, University of California, San Diego, 9500 Gilman Drive, La Jolla, CA 92093, USA.

P. Puhl-Quinn, EOS, University of New Hampshire, Durham, NH 03824, USA.